NATIONAL ADVISORY COMMITTEE FOR AERONAUTICS

TECHNICAL NOTE 3564

EFFECT OF PNEUMATIC DE-ICERS AND ICE FORMATIONS ON AERODYNAMIC CHARACTERISTICS OF AN AIRFOIL

By Dean T. Bowden

Lewis Flight Propulsion Laboratory
Cleveland, Ohio

NACA

Washington
February 1956

NATIONAL ADVISORY COMMITTEE FOR AERONAUTICS

TECHNICAL NOTE 3564

EFFECT OF PNEUMATIC DE-ICERS AND ICE FORMATIONS ON AERODYNAMIC CHARACTERISTICS OF AN AIRFOIL

By Dean T. Bowden

SUMMARY

Measurements of lift, drag, and pitching moment of an NACA 0011 airfoil were made in icing using two types of pneumatic de-icers, one having spanwise inflatable tubes and the other having chordwise tubes. Ice remaining after inflation of the spanwise-tube de-icer increased airfoil section drag 7 to 37 percent for 0° to 4.6° angle of attack over the ranges of airspeed, total air temperature, liquid-water content, and cycle times covered. This drag increase became constant after a few de-icing cycles. Drag increases due to ice remaining on the chordwise-tube de-icer were similar to those for the spanwise-tube de-icer. Minimum airfoil drag in icing (averaged over a de-icing cycle) was usually obtained with a short (about 1 min) de-icing cycle.

Alternate tube inflation was normally used, whereby every other tube was inflated and deflated, followed by inflation and deflation of the remaining tubes. In dry air, alternate inflation of the spanwise boot increased airfoil drag (averaged over a 1-min cycle) by 10 to 16 percent. Simultaneous tube inflation reduced the 10-percent increase to 3.2 percent. Inflating the chordwise boot had a negligible effect on average airfoil drag.

With the de-icer inoperative, rime-ice formations of 0.5 pound per foot span increased airfoil section drag 38 to 67 percent and decreased lift up to 4 percent for 0° to 4.6° angle of attack. The same amount of ridge-type glaze ice increased drag 124 to 230 percent and decreased lift up to 20 percent for 0° to 9.3° angle of attack. To help determine the effect of size and location of ridge-type ice formations on drag, spanwise spoilers were mounted on the bare airfoil at various chordwise positions. From these data, the drag increase was found to vary almost directly with spoiler height and the local air velocity over the bare airfoil.

INTRODUCTION

Ice formations on aircraft wings can be removed by heating the surfaces, by mechanical removal systems, or by chemical means (freezing-point depressants). Previous NACA icing investigations have been concerned largely with thermal methods of ice protection. The present study is an investigation of the pneumatic-boot mechanical de-icing system.

Pneumatic de-icers have several advantages over thermal de-icing systems. The air flow required for operation of the pneumatic system is very small compared with flow rates for a hot-gas de-icing system. Also, pneumatic de-icers may be added to an existing aircraft with little difficulty, whereas a hot-gas system must be designed and built as part of the original aircraft structure. A cyclic electric de-icing system generally is heavier and consumes much more power than the pneumatic system. The total weight of a cyclic electric system for an interceptor aircraft is shown in reference 1 to be 269 pounds compared with 79 pounds for the pneumatic system.

Pneumatic de-icer boots have long been used to de-ice the wing and tail surfaces of aircraft. The early de-icers, which operated at low inflation pressures, had several large inflatable tubes running spanwise along the airfoil leading-edge section. Ice formations were removed by periodic inflation and deflation of the de-icer tubes accomplished by alternate applications of air pressure and vacuum to the tubes. The boots were secured to the airfoil by spanwise metal strips.

As aircraft speeds increased, operational difficulties with the early boots were encountered, and improved de-icing performance was sought. In areas of low static pressure over the airfoils, autoinflation of the tubes occurred and disrupted the air flow over the surfaces. Lifting of the entire boot away from the airfoil surfaces also occurred during certain phases of operation. During the inflation portion of the cycle, large drag increases and lift decreases occurred because of the spoiler action of the large inflated tubes. In addition, the de-icing performance of the boots was not always reliable, and occasionally an ice cap would not be shed from the wing leading edge.

To reduce the aerodynamic effects during boot inflation and to improve the de-icing effectiveness, a new type pneumatic de-icer boot was developed by the manufacturer. The new-style boot, currently in use on some transport aircraft, consists of a large number of small spanwise tubes operating with a high inflation pressure (ref. 2). A high vacuum source is used to prevent autoinflation of the tubes during the deflation period, and cementing the boot to the airfoil surface eliminates the boot-lifting problem. The large number of small tubes are used to reduce the lift and drag penalties during inflation because of the reduced spoiler effect of the small tubes. The small tubes also improve

the de-icing performance by providing a greater local surface curvature during inflation to aid in cracking the ice from the boot, as well as providing more points for ice fracture.

Pneumatic boots with spanwise inflation tubes may cause buffeting when located ahead of control surfaces. To eliminate this problem, another boot, consisting of small tubes running chordwise from the leading edge, was recently developed. The use of chordwise tubes should greatly reduce the aerodynamic penalties during tube inflation. It is possible, however, that de-icing difficulties may arise near the leading edge where the surface curvature may prevent sufficient stretching of the tubes.

Several previous aerodynamic studies have been made to determine the drag increase of de-icer boots installed on smooth airfoils (refs. 3 and 4). Drag increases in dry air for inflation of the old-style boots are shown in reference 3, but drag data with boots inflated are not available for the new type boots now in use. No data exist on the aerodynamic penalties associated with cyclic operation of the boots in icing conditions. Penalties due to ice remaining on the boots after inflation have not been previously assessed. Drag increase resulting from such residual ice may persist for a considerable period of time after the aircraft emerges from icing conditions because of the slow removal of ice by sublimation. The effectiveness of pneumatic de-icers can best be obtained by comparing the aerodynamic penalties in icing conditions for an unprotected airfoil surface with an airfoil equipped with a boot. Drag penalties for unprotected airfoils in icing conditions are given in references 5 and 6, but lift and pitching moment were not measured.

A better understanding of the performance and penalties of pneumatic de-icers in icing conditions would aid in selecting ice-protection systems for aircraft under development and in the operation of de-icer boots already installed on aircraft. For these reasons, the present study was conducted in the NACA Lewis laboratory icing tunnel using an NACA 0011 airfoil equipped with both spanwise- and chordwise-tube de-icer boots. The objectives of the investigation were to determine the effects of (1) primary and residual ice formations on airfoil lift, drag, and pitch, (2) boot installation and inflation on airfoil lift and drag, and (3) various cycles, sequences, and methods of de-icer operation on airfoil drag. Aerodynamic effects of primary ice formations by means of spoilers were also studied.

SYMBOLS

C_D airfoil section drag coefficient, dimensionless

C_L airfoil lift coefficient, dimensionless

$C_{m_{c/4}}$ pitching-moment coefficient about quarter-chord point, dimensionless

c airfoil chord, ft

p static pressure, lb/sq ft

q dynamic pressure, lb/sq ft

Subscripts:

i refers to initial conditions (clean airfoil, boot deflated)

l local conditions at airfoil surface

∞ free-stream conditions

DESCRIPTION OF MODEL AND EQUIPMENT

The model used in this study was an NACA 0011 airfoil of 87.4-inch chord, spanning the 6-foot height of the 6- by 9-foot icing research tunnel (fig. 1). The airfoil was equipped with a 4-foot-span pneumatic-boot de-icer cemented to a removable leading-edge section of the airfoil. The entire airfoil, with the exception of the area covered by the de-icer, was steam-heated to prevent the accumulation of frost due to tunnel air turbulence and supersaturation. Two de-icers were tested, one having spanwise inflatable tubes and the other having chordwise tubes. The tube arrangement and chordwise extent of the two de-icers are shown in figure 2.

The chordwise extent of the inflatable area of the spanwise-tube de-icer was 7 inches on the upper surface and 11.5 inches on the lower surface. Aft of the inflatable part of the boot, on both surfaces, was a 3-inch tapered area that faired the de-icer into the airfoil shape (fig. 3). The upper surface had one 1.25-inch-wide tube at the leading edge, two 1-inch tubes, and five 0.75-inch tubes; while the lower surface had one 1.25-inch, two 1-inch, and eleven 0.75-inch tubes. The last six tubes on the lower surface could be controlled as a unit independently of the other tubes. Air for tube inflation was supplied through a chordwise manifold located near the tunnel-floor end of the boot. The manifold was connected to a vacuum source for the deflated condition to avoid bulging in areas of low local static pressure on the airfoil surface. The boot was constructed to allow alternate tube inflation; the "A" set of tubes (see figs. 2 and 3) were inflated first, then allowed to deflate while the "B" tubes were inflated. The tubes could also be inflated simultaneously when desired.

The chordwise-tube de-icer was similar in construction and over-all dimensions to the spanwise-tube de-icer. The chordwise extent of inflatable area was the same for both boots. The inflatable area of the chordwise boot consisted of 45 1-inch tubes, which were supplied with air from a spanwise manifold located on the boot lower surface. Alternate tube inflation was used on this boot also.

A timer-operated solenoid distributing valve controlled the air and vacuum supplies to the boot. This valve normally allowed a vacuum of 6 inches of mercury to be applied to the tubes. Energizing the A solenoid on the valve changed the boot A inlet from vacuum to pressure, and the A tubes were inflated. After the A tubes were inflated, the solenoid was de-energized, and the air in the boot discharged to the atmosphere through a vent in the distributing valve. When the boot pressure was near ambient, the port was connected to the vacuum, and deflation was completed. The B tubes were inflated immediately after the A solenoid was de-energized.

Air at 22 pounds per square inch was normally supplied to the distributing valve from a throttling valve connected to a high-pressure air source. For some of the tests, however, the inflation air pressure was varied from 15 to 40 pounds per square inch. Vacuum for boot deflation was supplied by an ejector operating continuously from the high-pressure air source and was controlled by a vacuum regulator. The distributing valve was connected to the boot by flexible air lines about 10 feet long and 5/8-inch inside diameter. All components of the air and vacuum systems were standard aircraft parts for the pneumatic boot de-icer.

The airfoil model was attached to the tunnel balance frame by a mounting plate welded to the bottom of the airfoil. The balance frame was connected to a six-component force balance system. Small air gaps were left between the airfoil and the tunnel ceiling and between the mounting plate and turntable to isolate the model from all but aerodynamic forces. The forces on the airfoil were recorded simultaneously by an electrically controlled printing mechanism at each balance scale.

Airfoil drag was also measured by means of an electrically heated wake survey rake located 1/4-chord downstream of the airfoil at midspan (fig. 1(a)). The rake had 80 electrically heated total-pressure tubes spaced on 1/4-inch centers and five static-pressure tubes spaced on 5-inch centers. Airfoil pressure distribution was measured at two spanwise locations (midspan and 25 in. above midspan) by means of pressure belts. All pressure data were photographically recorded from multitube manometers.

Liquid-water content was measured by means of a pressure-type icing-rate meter (ref. 7). Icing-cloud droplet size was obtained from a previous calibration obtained by using water droplets carrying dye in solution (ref. 8).

CONDITIONS AND PROCEDURES

The investigation was conducted under the following conditions:

Nominal airspeed, mph	175 and 275
Nominal Reynolds number, dimensionless	12 and 19×10^6
Angle of attack, deg	0 to 9.3
Air total temperature, ^{o}F	0 to 30
Liquid-water content, g/cu m	0.3 to 1.0
Volume-median droplet diameter, microns	7 to 14
Maximum droplet diameter, microns	22 to 50
Icing period, min	0.9 to 3.9

The tube inflation time for both de-icers was kept constant at 3 seconds per set of tubes, or 6 seconds total for alternate inflation and 3 seconds total for simultaneous inflation. The 3-second period was chosen as representative of most boot installations. The time required for complete inflation may be more or less than 3 seconds, depending on boot capacity. Cycle time, which is defined as the time from the start of one inflation period to the start of the next, was varied from 1 to 4 minutes.

To study the effects of residual ice on lift, drag, and pitch, a particular icing condition and de-icing cycle were set, and the model was allowed to ice and de-ice for about 30 minutes. During this period, data were normally taken before and after ice removal for each de-icing cycle. Photographs of both airfoil surfaces were usually taken before and after ice removal for one de-icing cycle after conditions were stabilized.

Icing runs with the boot inoperative (deflated) were made to determine the effects of primary ice on airfoil aerodynamic characteristics. The airfoil was allowed to collect ice for 15 to 30 minutes, depending on the icing rate, and data were recorded at 1- to 4-minute intervals. Photographs were taken at frequent intervals to record ice size and shape. The amount of ice collected was estimated from experimental impingement data. The rate of collection was assumed constant with time in icing.

Before measuring the airfoil drag with the boot removed, the aluminum leading-edge section was carefully sanded to remove any surface imperfections. To aid in analyzing the effects of ice on airfoil lift and drag, spoilers were added to the airfoil by cementing 1/4- by 1/2- or 1/2- by 1/2-inch rubber strips 4 feet long at various chordwise positions.

The effect of air gaps at the ends of the airfoil on drag measured by the balance system was determined by comparing the rake and balance-system drag coefficients obtained in dry air. Airfoil drag measured by

the balance system was higher than that measured by the rake located at midspan, probably because of increased drag at the ends of the airfoil resulting from the air gaps. A spanwise survey using a small movable rake also was made. The average drag for the 4-foot boot section was essentially equal to the drag measured at the center of the tunnel. Near the tunnel floor and ceiling, however, the drag increased considerably over the center-section value. Increases in drag (due to de-icer inflation or to addition of spanwise spoilers) measured by the balance system, however, were the same as for the rake at midspan. It was concluded that the drag coefficients for the clean airfoil should be based on the rake, but that drag increases measured by the balance system were valid. All drag increases shown, therefore, were obtained from the balance system, while initial drag values were obtained from the rake.

Airfoil end effects on lift and pitching moment were also evaluated for the clean airfoil. Airfoil lift and pitching moment were calculated from the experimentally determined pressure distribution and were compared with corresponding balance-system data. Good agreement was obtained, indicating that, for the gap size and angle of attack range covered (0° to 9.3°), the airfoil end effects on lift and pitching moment were not significant.

All data presented are corrected for tunnel-wall interference effects by use of the equations of reference 9. Drag coefficients in previous icing-drag reports (refs. 5 and 6) were not corrected for wall interference.

RESULTS AND DISCUSSION

The results are presented in two sections, the first of which is concerned with airfoil characteristics with the de-icer operating. The effects of residual ice, boot installation, and tube inflation on airfoil characteristics are presented. From these data, de-icing cycles are determined for minimum airfoil drag in icing. The effects of various methods of boot operation on ice removal are shown. In most cases, data are presented for both the spanwise- and chordwise-tube de-icers.

The second section shows the effect of primary ice formations on airfoil characteristics with the de-icer inoperative. Airfoil drag increases resulting from ice formations are correlated with size of ice accumulation for several types of ice. The aerodynamic effects of ridge-type glaze-ice formations are studied with the use of spanwise spoilers.

In the following discussion all aerodynamic characteristics are presented in coefficient form. All drag values given are airfoil section drag and do not include induced drag. Airfoil section drag may be only 1/8 to 1/3 of aircraft total drag, depending on aircraft configuration and operating conditions.

Airfoil Characteristics with De-Icer Operating

Typical de-icing characteristics of pneumatic de-icers. - Photographs showing typical de-icing performance of the spanwise- and chordwise-tube de-icers are shown in figures 4 and 5 for various icing and operating conditions. Boot inflation usually removes the main part of an ice formation but leaves small flakes of ice on the boot. Consequently, airfoil drag after boot inflation is somewhat greater than the clean-airfoil drag. In glaze-icing conditions (figs. 4(c) and (d)), the spanwise de-icer usually removes ice more completely than in rime-icing conditions (figs. 4(a) and (b)). De-icing performance of the chordwise boot (fig. 5) is similar to that of the spanwise boot.

Typical variation of drag, lift, and pitching moment with icing time is shown in figure 6 for two rime-icing conditions with the spanwise boot operating. The low icing rate of figure 6(a) increases airfoil drag very little during the icing period. After boot inflation, the small amount of residual ice left on the boot has little effect on drag. Increasing the icing rate and angle of attack (fig. 6(b)) increases the rate of drag increase during the icing period. After ice removal, the drag is higher than in figure 6(a) because of the increased chordwise extent of residual ice.

Variation of airfoil characteristics in glaze-icing conditions is shown for the spanwise boot in figure 7 for two icing periods. Airfoil drag increases rapidly during the icing period of figure 7(a) but decreases to near the clean-airfoil value after ice removal. Airfoil drag immediately following ice removal is constant regardless of time in icing. For comparison, airfoil drag with the boot inoperative is also shown in figure 7(a). After 16 minutes icing time, airfoil drag has increased 250 percent with the boot inoperative, whereas the drag increase is only 24 percent after 16 minutes in icing with the boot operating.

Airfoil drag with the boot inflated is also shown in figure 7(a). Boot inflation increases drag about 105 percent for this angle of attack (2.3°) in both dry air and icing. A detailed study of lift, drag, and pitching-moment changes resulting from boot inflation was made in dry air, as will be discussed later.

For high icing rates such as that of figure 7(a), a shorter cycle time would be desirable to reduce average airfoil drag in icing. Airfoil characteristics are shown in figure 7(b) for a 1-minute cycle time at the same icing conditions as figure 7(a). The drag coefficient before ice removal is about 0.0099 for the 1-minute cycle, compared with about 0.0122 for the 4-minute cycle. After ice removal, the drag coefficient is about the same for both de-icing cycles.

Effect of residual ice on drag and lift. - The drag increase resulting when ice remains on the airfoil after boot inflation is significant as a measure of de-icer effectiveness. This drag increase also represents the drag penalty that continues after an aircraft emerges from an icing encounter.

The effect of icing period on ice-removal effectiveness of the spanwise-tube de-icer was studied for various cycle times over a wide range of operating conditions. The drag increase due to ice remaining after inflation was used as a measure of de-icing performance. Ice removal sometimes appeared to improve slightly when the icing period was increased. The drag after removal, however, did not vary appreciably with icing period for the range covered in the tests (0.9 to 3.9 min).

The effect of residual ice on lift and drag is shown in figure 8 as a function of lift coefficient for the spanwise de-icer. Each lift or drag data point shown represents an average value for several cycles. The drag coefficient after ice removal varies with chordwise extent of residual ice, angle of attack, and with liquid-water content at high angles of attack. Air total temperature apparently has no consistent or significant effect on drag after ice removal in the range investigated (0° to 30° F). For a liquid-water content of 0.5 gram per cubic meter and airspeed of 175 miles per hour (fig. 8(a)), residual ice increases drag about 7 to 14 percent over the clean-airfoil drag. For this airspeed and a higher liquid-water content (1.0 g/cu m), however, the drag increases are greater. At a lift coefficient of 0.4, the drag increase is 15 percent for 1.0 gram per cubic meter, compared with 9 percent for a liquid-water content of 0.5 gram per cubic meter. The difference is a result of increased surface extent of residual ice due to impingement farther aft with the increased maximum water-droplet size. In the icing tunnel, droplet size increases with liquid-water content for a particular airspeed (ref. 8). For lift coefficients of 0.6 to 0.8, the drag increase at 1.0 gram per cubic meter is 50 to 100 percent. Although ice removal appeared to be good for this condition, small spanwise ridges of ice were left on the airfoil near the leading edge. At high angles of attack, these ridges could cause large drag increases if located on the upper surface (ref. 5).

At the higher liquid-water content (1.0 g/cu m), losses in lift due to residual ice varied from 5 to 13 percent for lift coefficients from 0.4 to 0.8. Residual ice had little effect on lift for the lower liquid-water content (0.5 g/cu m).

For a given liquid-water content, drag increases due to residual ice were generally greater for an airspeed of 275 miles per hour (fig. 8(b)) than for 175 miles per hour (fig. 8(a)). The larger drag increase at 275 miles per hour is a result of greater extent of residual ice due

to increased maximum water-droplet size and higher airspeed. In the icing tunnel, droplet size increases with water flow rate. The water flow rate must be increased with airspeed to maintain a given liquid-water content; consequently, droplet size increases with airspeed for a constant water content. At 275 miles per hour, drag increase due to residual ice varies from 23 to 37 percent, compared with 7 to 14 percent for 175 miles per hour.

Airfoil drag with standard roughness (ref. 10) is shown in figure 8 for comparison. Standard roughness consisted of 0.00046-chord grains distributed from the airfoil leading edge to 0.08 chord on both surfaces. With the exception of data at high angle of attack and high liquid-water content, airfoil drag with residual ice is generally less than with standard roughness. Drag of the smooth airfoil of reference 10 is lower than that of the present clean airfoil. This difference is probably due to the presence of the de-icer boot and to the higher turbulence level in the icing tunnel.

Generally, the ice-removal characteristics of the chordwise-tube de-icer were similar to those of the spanwise de-icer. The drag increase due to residual ice on the chordwise de-icer is shown in figure 9 for two airspeeds. The drag increase at 275 miles per hour is the same for both boots. At the lower airspeed, residual ice increases drag about 15 percent for the chordwise boot, compared with 7 to 14 percent for the spanwise boot.

The drag increase due to residual ice may be correlated with chordwise extent of the ice for the lower angles of attack (0° to 4.6°). The increase in drag (fig. 10) increases directly with chordwise extent of residual ice and is not affected appreciably by airspeed, angle of attack, air temperature, or liquid-water content, except as they affect chordwise extent of residual ice. This relation should be useful in estimating drag increases due to residual ice for conditions not covered by the present tests and for other boot-equipped airfoils of similar thickness. Extent of residual ice may be calculated from airfoil impingement data, which are now available for a variety of airfoils.

Comparison of pneumatic de-icer with thermal de-icing system. - A thermal de-icing system, such as the one used in reference 5, usually produces runback icing behind the heated area. This runback increases airfoil drag and may be compared with the residual ice that increases airfoil drag with the pneumatic de-icer. In rime-icing conditions, small amounts of runback from the thermal system (ref. 5) had little effect on drag, whereas residual ice from the pneumatic de-icer increased drag 7 to 37 percent. In heavy glaze-icing conditions, however, airfoil drag after ice removal increased with icing time for the thermal system and remained constant for the pneumatic de-icer. A comparison of airfoil drag increase for the two types of de-icing systems is shown in

figure 11 for heavy glaze-icing conditions. Although the test conditions were not identical, the icing rates were similar for the two cases. This comparison shows that drag after ice removal for a thermal system may become greater after several de-icing cycles than for the pneumatic de-icer. Figure 11 illustrates only one case for comparison purposes, and it may not be typical. Other airfoil shapes, test conditions, heating rates, and system designs might greatly alter the comparison.

Airfoil drag increase due to de-icer installation. - A de-icer installation that increases airfoil drag will affect aircraft performance even though icing conditions are not encountered. The addition of old type boots to a smooth airfoil (ref. 3) increased airfoil drag by 13 to 29 percent. Installation of present-day de-icer boots increased airfoil drag 12 to 23 percent for one smooth airfoil, and 25 to 100 percent for another (ref. 4). Both the airfoils shown in reference 4 had a drag coefficient of about 0.0070 with the present type of boots attached. However, some of the practical construction airfoils tested in reference 4 having surface irregularities but no de-icer boots had drag coefficients equal to or greater than 0.0070.

The drag coefficient of the present airfoil with boot attached is also about 0.0070 for the same lift coefficient as the tests of reference 4 ($C_L = 0.3$). Removing the boot from the present airfoil, however, had no effect at 275 miles per hour and reduced drag less than 5 percent at 175 miles per hour (fig. 12). Present airfoil drag with the boot attached is about 15 to 30 percent higher than drag of the smooth airfoil of reference 10, obtained in a low-turbulence tunnel. The higher turbulence of the icing tunnel and the surface imperfections on the present airfoil probably are responsible for the difference between the present bare-airfoil drag (boot removed) and the airfoil drag from reference 10.

The drag increase due to installation of de-icers will vary widely, depending on airfoil type and surface condition, operating conditions, and type of boot installation. Adding boots to a smooth airfoil could increase drag 12 to 100 percent, while adding boots to an airfoil having surface irregularities could have little or no effect on drag.

Effect of boot inflation on airfoil characteristics. - Airfoil drag with the boot inflated as well as drag during the icing period must be known in order to determine the cycle that will yield minimum drag for a particular icing and operating condition. Inasmuch as airfoil characteristics at the moment of inflation of the spanwise boot were about the same in dry air as in icing, a study of boot-inflation effects on airfoil characteristics was made in dry air with both the spanwise- and chordwise-tube de-icers.

Airfoil characteristics with the spanwise boot inflated are shown in figure 13 for two airspeeds. The increase in drag due to boot inflation varies from about 100 to 165 percent at an airspeed of 175 miles

per hour (fig. 13(a)). The greatest drag increase is obtained at the highest value of lift coefficient. Airfoil drag with B tubes inflated is slightly higher than with A tubes inflated. Leaving the last six tubes on the lower surfaces deflated decreased the boot-inflated drag only a small amount. Boot inflation decreased lift 6 to 10 percent for a range of angles of attack from 2.3° to 9.3°. Pitching-moment coefficient increased linearly from 0 to 0.015 with increasing angle of attack. Similar results are shown in figure 13(b) for an airspeed of 275 miles per hour and a range of angles of attack from 0° to 4.6°. One data point was obtained at 2.3° angle of attack with all tubes inflated simultaneously. The drag increase for simultaneous tube inflation was only 65 percent compared with 120 percent for alternate tube inflation. With all tubes inflated the forward part of the airfoil is thickened slightly, but the surface is not so discontinuous as with alternate inflation.

The drag increase due to inflation of the chordwise-tube de-icer was also obtained in dry air (fig. 14). Inflating the boot increases drag only 5 percent and has no effect on lift. Inflation of the chordwise tubes forms ridges parallel to the airstream that have much less effect on drag than the spanwise ridges formed by inflation of the spanwise tubes. The drag increase for inflation of the chordwise boot was substantiated by comparison with the data of reference 11. These data show that the drag increase due to chordwise protrusions is proportional to twice the increase in surface area. The increase in exposed surface due to inflation of the chordwise boot is 1.8 percent. Thus, the predicted increase in drag is 3.6 percent compared with the measured value of 5 percent.

The drag increase due to inflation, averaged over a complete cycle, would be only 1/10 to 1/40 of the values shown in figures 13 and 14 (assuming 6 sec inflated, and 0.9 to 3.9 min deflated). Values of the average drag increase due to de-icer operation in dry air are shown in figure 15. Alternate inflation of the spanwise boot increased the average drag 10 to 16 percent for a 1-minute cycle, but only 2.5 to 4 percent for a 4-minute cycle. The drag increase with simultaneous tube inflation is considerably lower; for a 1-minute cycle and 2.3° angle of attack, the increase in average drag is 3.2 percent compared with 10 percent for alternate tube inflation. The lower drag is a result of reduction in both instantaneous drag due to inflation and in inflation time. Inflation of the chordwise boot caused a negligible increase in average airfoil drag.

Average airfoil drag in icing with boot operating. - For a particular icing and operating condition, the de-icing cycle should be selected so that airfoil drag averaged over a cycle is a minimum. Inasmuch as inflation of the chordwise boot had a negligible effect on airfoil drag, the shortest de-icing cycle used (1 min) always yielded the minimum average airfoil drag in icing for the chordwise boot. For the spanwise boot, however, average drag in icing must be evaluated to determine the optimum

cycle for a given icing and operating condition. Average drag increase in icing was determined for the spanwise boot from figure 16 and other similar plots. These drag increases for a variety of icing conditions are plotted in figure 17 as a function of cycle time. For the lower ice-accretion rates, the average drag increase reduces slightly with increasing cycle time. The difference in drag increase between 4- and 1-minute cycles, however, is only 2 to 6 percent. For higher ice-accretion rates, the average drag increase is greater for the longer cycles. For an ice-accretion rate of 4.8 pounds per hour per foot span and glaze-icing conditions, the drag increase for the 4-minute cycle is double that for a 1-minute cycle. A fixed de-icing cycle is often desired to simplify de-icer controls. Where this is the case, the short cycle (1 min) represents the best compromise for the spanwise de-icer.

Effect of various modes of boot operation on ice removal. - The effects on ice removal of (1) inflation air pressure, (2) simultaneous tube inflation, (3) increased air-supply-line length, and (4) a coating that reduces ice adhesion were investigated with the spanwise-tube de-icer.

For one rime-icing condition at an airspeed of 275 mph and angle of attack of 2.3°, the inflation air pressure was varied from 15 to 40 pounds per square inch. The ice removal appeared to be slightly better at 22 than at 15 pounds per square inch and about the same at 30 and 40 as at 22 pounds per square inch. Airfoil drag after removal was essentially constant regardless of inflation air pressure. It may be concluded that inflation air pressure does not have a significant effect on ice-removal effectiveness for the range from 15 to 40 pounds per square inch for this installation.

Ice-removal characteristics and drag after removal were studied for one icing condition with simultaneous inflation and were found to be the same as with alternate inflation. Simultaneous tube inflation has several advantages over alternate inflation. First, the average drag increase with simultaneous inflation is about one-third of that for alternate inflation (fig. 15). Second, the amount of air-supply hose from the distributing valve is reduced by half, as only one connection per boot is required, rather than two. Also, the boot manifold size is reduced by half. The only disadvantage is that the instantaneous air-flow rate is doubled. Where the available air supply permits, simultaneous tube inflation should be considered for the spanwise boot.

In cases where space and accessibility are critical, it might be desirable to locate the air-distributing valves within the aircraft fuselage rather than close to each boot. However, the long lines required for such an installation might have adverse effects on ice removal. De-icing tests were made with 40 feet of air-supply line added to the existing lines, making a total length of over 50 feet. The time required for

boot deflation increased with the longer lines, but no effect on time for inflation was apparent. The drag after ice removal, however, was the same with the 50-foot supply lines as with the short supply lines.

A coating to reduce ice adhesion, which was supplied by the de-icer boot manufacturer, was tested briefly. The first tests were made with the lower half of the boot coated. The coated half of the boot shed considerably more ice than the untreated half (fig. 18). The entire boot was then coated, and data were obtained for several de-icing cycles. The average drag increase due to residual ice was 17 percent, compared with about 40 percent for the untreated boot. After seven cycles, the drag after ice removal was still approximately the same as for the first cycle. Since some of the coating is removed at each inflation, the coating will eventually wear off and have to be replaced. Tests were not made in the icing tunnel to determine the time required for the coating to wear off. However, data presented in reference 12 show that after 26 de-icing cycles all the coating was removed, and the ice adhesion forces were the same as for the untreated rubber surface. Flight through rain may also remove part of the coating, reducing its effectiveness. For small airplanes where the airfoil surfaces are easily accessible, the coating should be useful. For large aircraft, the difficulty and expense of applying and renewing the coating might outweigh the improvement in ice removal.

Effect of Primary Ice Formations on Drag, Lift, and Pitch with De-Icer Inoperative

Airfoil characteristics in icing with the de-icer operating have been discussed. The need for a de-icing system can be determined for a particular aircraft and flight plan if the aerodynamic penalties incurred in icing conditions with no protection are known. This section presents airfoil lift, drag, and pitch in icing with the de-icer inoperative. The aerodynamic effect of ice-formation height and location is also determined by means of spanwise spoilers.

Typical primary ice formations. - Typical rime-ice formations, characteristic of the lower air temperatures and icing rates, are shown in figure 19. The formations are relatively streamlined and, for icing times of 11 to 15 minutes, increase airfoil drag 11 to 36 percent, depending on the size of the ice formation. The ice formation in figure 19(b) is about 3 times as large, on a calculated weight basis, as that of figure 19(a), and the drag increase (36 percent) is about 3 times as great.

At a low air temperature and high liquid-water content, a glaze-rime-ice formation, such as that shown in figure 20, may result. Glaze

ice forms in the heavy impingement region near the leading edge. Farther back on the airfoil, rime ice forms where impingement rates are low. This ice formation increased airfoil drag 120 percent and decreased lift 8 percent.

Typical glaze ice, formed at a high air temperature and moderate icing rate, is shown in figure 21. The ice formation is slightly rougher and more irregular than that of rime ice (fig. 19). This glaze-ice formation increases airfoil drag 45 percent and decreases lift 3 percent.

Ridge-type glaze-ice formations (fig. 22), which form at high air temperature (25° F) and high icing rates, cause large increases in drag and losses in lift. At a low angle of attack (fig. 22(a)), two distinct ridges, one on the upper surface and one on the lower, may be seen. For the higher angle of attack (fig. 22(b)), a distinct ridge is formed only on the upper surface. The formation of figure 22(a) increases drag 275 percent, while that of figure 22(b) increases drag 200 percent. Both formations decrease lift 11 percent.

Variation of drag, lift, and pitch with icing time. - The effect of rime-ice formations on airfoil characteristics is shown as a function of icing time in figure 23 for two conditions. The drag in figure 23(a) increases only 20 percent in 16 minutes because of the low rate of ice accretion. Changes in lift and pitch for figure 23(a) are negligible.

The higher ice-accretion rate and angle of attack of figure 23(b) result in a drag increase of 73 percent in 16 minutes, but only a 3- to 4-percent loss in lift. Lift decreases slightly at first, then becomes practically constant. Pitching-moment coefficient increases slightly (0.004) in the first 2 minutes and is constant thereafter.

The aerodynamic penalties are much more severe for ridge-type glaze ice than for rime ice. Glaze ice that forms spanwise ridges on the airfoil disrupts the flow and may cause flow separation. The drag increase for the ridge-type glaze ice of figure 24(a) is 253 percent in 16 minutes, compared with 73-percent increase for the same exposure to rime-icing conditions (fig. 23(b)). Ridge-type glaze ice at 7.0° angle of attack (fig. 24(b)) increases drag 220 percent, reduces lift 11 percent, and increases pitching-moment coefficient by 0.02 in only 12 minutes. Prolonged flight in icing conditions similar to those of figure 24 would require some form of icing protection. The need for protection for short icing exposures and in milder icing conditions should be determined by operational analyses of the present and similar data for each specific problem area.

Correlation of drag and lift changes with size of ice formation. - The increase in airfoil drag due to an ice formation is a function of the size, shape, and location of the ice, and of airfoil angle of attack. For a given type and shape of ice formation, it should be possible to

correlate drag and lift changes as a function of amount of ice accumulated at a particular angle of attack. Accordingly, airfoil drag and lift changes due to primary ice formations are plotted in figure 25 against ice accumulation for 0° to 9.3° angles of attack. The amount of ice collected was calculated from experimental impingement data. Airfoil collection efficiency was assumed constant with time in icing. For rime-ice formation, 0.5 pound per foot span of ice increases drag 38 to 67 percent and decreases lift up to 4 percent for angles of attack from 0° to 4.6°. The same amount of ridge-type glaze ice increases drag 124 to 230 percent and decreases lift up to 20 percent for angles of attack from 0° to 9.3°. The drag increase with light glaze ice is no greater than with rime ice. Drag increase with a glaze-rime-ice formation is greater than for rime but less than for ridge-type glaze ice.

The drag data of figure 25 are cross-plotted in figure 26 against angle of attack for rime and ridge-type glaze ice. With rime ice the drag increase is constant from 0° to 2°, then increases from 2° to 5°. The drag increase is roughly constant from 0° to about 6° angle of attack for ridge-type glaze ice but increases rapidly with angles of attack over 6°. The drag increase for 0.3 pound per foot span of ridge-type glaze ice is about the same as for 1.2 pounds per foot span of rime.

A small ice formation accumulated at low angle of attack can increase drag greatly when angle of attack is increased for landing. The data shown in figure 27 were obtained by allowing ice to accumulate for 12 to 28 minutes at 0°, 2.3°, or 4.6° angle of attack and then increasing the angle to simulate a landing approach. Rime ice that formed at 0° angle of attack at 275 miles per hour increased drag by about 25 percent. Increasing the angle to 4.6°, however, resulted in a drag increase of 122 percent of the bare airfoil drag at 4.6°, compared with a 65-percent increase for the same amount of ice accumulated at 4.6° (dashed curve, fig. 27). The drag curves for ice formed at 2.3° or 4.6° have the same typical shape as the curves for ice formed at zero angle of attack but are merely shifted to the right of them. Although maximum-lift data were not obtained, the shape of the lift curve at high angles of attack shows that a large loss in maximum lift may take place.

Explanation of aerodynamic effects of airfoil icing by use of rectangular spoilers. - A clear understanding of the aerodynamic effects of airfoil icing, as measured experimentally in icing conditions, is hampered by the complex shape of the ice. It is difficult to measure distances along the convolutions of ice growths and to determine which part of the ice formation is significant and which is incidental. Existing data indicate that ice constituting only a roughening of the surface may have a relatively small aerodynamic effect, while ridge-type ice resembling a surface protrusion or spoiler has much larger aerodynamic effects. To better understand the aerodynamic effects caused by protuberant ice, spanwise rectangular spoilers of two heights representative of ice-formation thicknesses were cemented to the airfoil at various chordwise

positions at which heavy ice accretions have been observed. By this means, the effect of spoiler heights and chordwise location as functions of angle of attack were determined. These effects are indicative of the aerodynamic effects obtained with actual ice formations, but not necessarily predictive of quantitative measurements.

The aerodynamic effects of 1/4-inch-high (0.00286-chord) spanwise spoilers at various chordwise locations are shown in figure 28(a). For the upper surface 5-percent-chord location, the present data are in good agreement with those of reference 13. The drag coefficients with spoilers at 1- or 2.5-percent chord are lower than those at 5-percent chord for low lift coefficients but are much higher at high lift coefficients. The drag coefficient with a spoiler on the lower surface decreases as the lift coefficient increases. Effects of spoilers on lift and pitching-moment coefficients are also shown in figure 28(a). Similar results obtained with 1/2-inch-high spoilers are shown in figure 28(b). Both the present data and those of reference 13 show that drag increase varies approximately linearly with spoiler height.

The effect of spoiler chordwise location on drag is shown in figure 29 by combining present data with that of reference 13. The drag increase with 1/4-inch-high spoilers is plotted against spoiler distance from the airfoil leading edge. On the lower surface, airfoil drag generally increases with spoiler chordwise distance from the leading edge. Spoilers located in the stagnation region apparently have little effect on airfoil drag. On the upper surface, drag increases with spoiler chordwise surface distance for 0° and 2.3° angle of attack. For the higher angles of attack, drag increases sharply from zero to about 1-percent chord and then decreases rapidly. The maximum drag increase usually occurs when the spoiler is mounted near the point of maximum local air velocity. The variation of local air velocity for the bare airfoil is shown in figure 30 by the plot of airfoil pressure distribution for two angles of attack. Maximum air velocity is obtained at the maximum negative value of pressure coefficient. The similarity in shape between the curves of figures 29 and 30 indicates that spoiler drag varies almost directly with the local air velocity distribution at the spoiler location.

The data of figure 27, for which the ice formations may be regarded as protuberances, are consistent with the data of figures 29 and 30. Although the ice shapes and locations were not precisely known, they were constant with angle of attack, and the drag trends were the same as with rectangular spoilers; namely, drag increases with angle of attack for protuberances close to the leading edge. As the angle of attack increases, the point of peak drag increase moves toward the airfoil zero-chord line (fig. 29). In this region, drag may increase from zero to a maximum of several times the bare-airfoil drag in a distance of less than

1 inch for the present airfoil. Because the drag of spoilers varies so rapidly in this region, an analysis of drag due to ice formations obviously requires precise measurements, including an average of the ice height and various shape factors not yet investigated.

Elsewhere over the airfoil and at lower angles of attack, the location of protuberances is not so critical. Reasonable predictions of drag of iced airfoils may be made from the spoiler data of reference 13 and the present investigation. Examples of predictions of this nature are given in reference 5.

SUMMARY OF RESULTS

The results of a study to determine the effects of pneumatic de-icers and ice formations on aerodynamic characteristics of an NACA 0011 airfoil may be summarized as follows:

1. Boot inflation removes the main part of an ice formation. Ice remaining after inflation of a spanwise-tube de-icer increased airfoil section drag 7 to 37 percent for the following conditions: angles of attack from 0° to 4.6°, airspeeds of 175 and 275 mph, glaze- and rime-icing conditions, air total temperatures from 0° to 30° F, liquid-water contents from 0.3 to 1.0 gram per cubic meter, and cycle times from 1 to 4 minutes. For these conditions the drag increase depended primarily on chordwise extent of residual ice. In heavy glaze-icing conditions (1.0 g/cu m liquid-water content and 25° F air total temperature) at high angles of attack (4.6° to 9.3°), ice remaining after inflation increased airfoil drag 15 to 100 percent. For a given operating condition, the drag increase due to residual ice usually was constant regardless of the number of de-icing cycles. Minimum airfoil drag in icing (averaged over a de-icing cycle) was usually obtained with a short (about 1 min) de-icing cycle. Alternate tube inflation of the spanwise de-icer in dry air increased airfoil section drag 100 to 165 percent and decreased lift 6 to 10 percent. Averaged over a 1-minute cycle, the drag increase with alternate inflation in dry air varied from 10 to 16 percent. Simultaneous tube inflation reduced the 10-percent increase to 3.2 percent.

2. Ice-removal characteristics of a chordwise-tube de-icer were the same as for the spanwise-tube de-icer. Minimum airfoil drag in icing using the chordwise de-icer was always obtained with a short (1 min) de-icing cycle. Inflation of the chordwise de-icer in dry air increased section drag only 5 percent, had no effect on lift, and had negligible effect on airfoil drag averaged over a cycle.

3. With the de-icer inoperative, rime-ice formations of 0.5 pound per foot span increased section drag 38 to 67 percent and decreased lift up to 4 percent for angles of attack from 0° to 4.6°. The same amount

of ridge-type glaze ice increased drag 124 to 230 percent and decreased lift up to 20 percent for angles of attack from 0° to 9.3°. Increasing the airfoil angle of attack with even a small ice formation on the airfoil can cause large increases in drag and losses in lift. Spanwise spoilers mounted at various chordwise positions were used to help determine the effect of size and location of ridge-type ice on airfoil drag. Such drag was found to vary almost directly with spoiler height and the local air velocity over the bare airfoil.

Lewis Flight Propulsion Laboratory
National Advisory Committee for Aeronautics
Cleveland, Ohio, November 23, 1955

REFERENCES

1. Miller, Ollie D.: Flight Test Results of the Goodrich High Pressure Pneumatic De-Icers. Tech. Note WCT-54-48, Wright Air Dev. Center, Wright-Patterson Air Force Base, July 1954.

2. Loughborough, Dwight L., Green, Howard E., and Roush, Paul A.: A Study of Wing De-Icer Performance on Mount Washington. Aero. Eng. Rev., vol. 7, no. 9, Sept. 1948, pp. 41-50.

3. Robinson, Russell G.: The Drag of Inflatable Rubber De-Icers. NACA TN 669, 1938.

4. Quinn, John H., Jr.: Summary of Drag Characteristics of Practical-Construction Wing Sections. NACA Rep. 910, 1948. (Supersedes NACA TN 1151.)

5. Gray, Vernon H., and von Glahn, Uwe H.: Effect of Ice and Frost Formations on Drag of NACA 65_1-212 Airfoil for Various Modes of Thermal Ice Protection. NACA TN 2962, 1953.

6. von Glahn, Uwe H., and Gray, Vernon H.: Effect of Ice Formations on Section Drag of Swept NACA 63A-009 Airfoil with Partial-Span Leading-Edge Slat for Various Modes of Thermal Ice Protection. NACA RM E53J30, 1954.

7. Perkins, Porter J., McCullough, Stuart, and Lewis, Ralph D.: A Simplified Instrument for Recording and Indicating Frequency and Intensity of Icing Conditions Encountered in Flight. NACA RM E51E16, 1951.

8. von Glahn, Uwe H., Gelder, Thomas F., and Smyers, William H., Jr.: A Dye-Tracer Technique for Experimentally Obtaining Impingement Characteristics of Arbitrary Bodies and a Method for Determining Droplet Size Distribution. NACA TN 3338, 1955.

9. Allen, H. Julian, and Vincenti, Walter G.: Wall Interference in a Two-Dimensional-Flow Wind Tunnel with Consideration of the Effect of Compressibility. Rep. 782, 1944. (Supersedes NACA ARR 4K03.)

10. Abbot, Ira H., and von Doenhoff, Albert E.: Theory of Wing Sections. First ed., McGraw-Hill Book Co., Inc., 1949.

11. Hoerner, S. F.: Aerodynamic Drag. Otterbein Press (Dayton), 1951.

12. Loughborough, D. L.: The Physics of the Mechanical Removal of Ice for Aircraft. Aero. Eng. Rev., vol. 11, no. 2, Feb. 1952, pp. 29-34.

13. Jacobs, Eastman N.: Airfoil Section Characteristics as Affected by Protuberances. NACA Rep. 446, 1932.

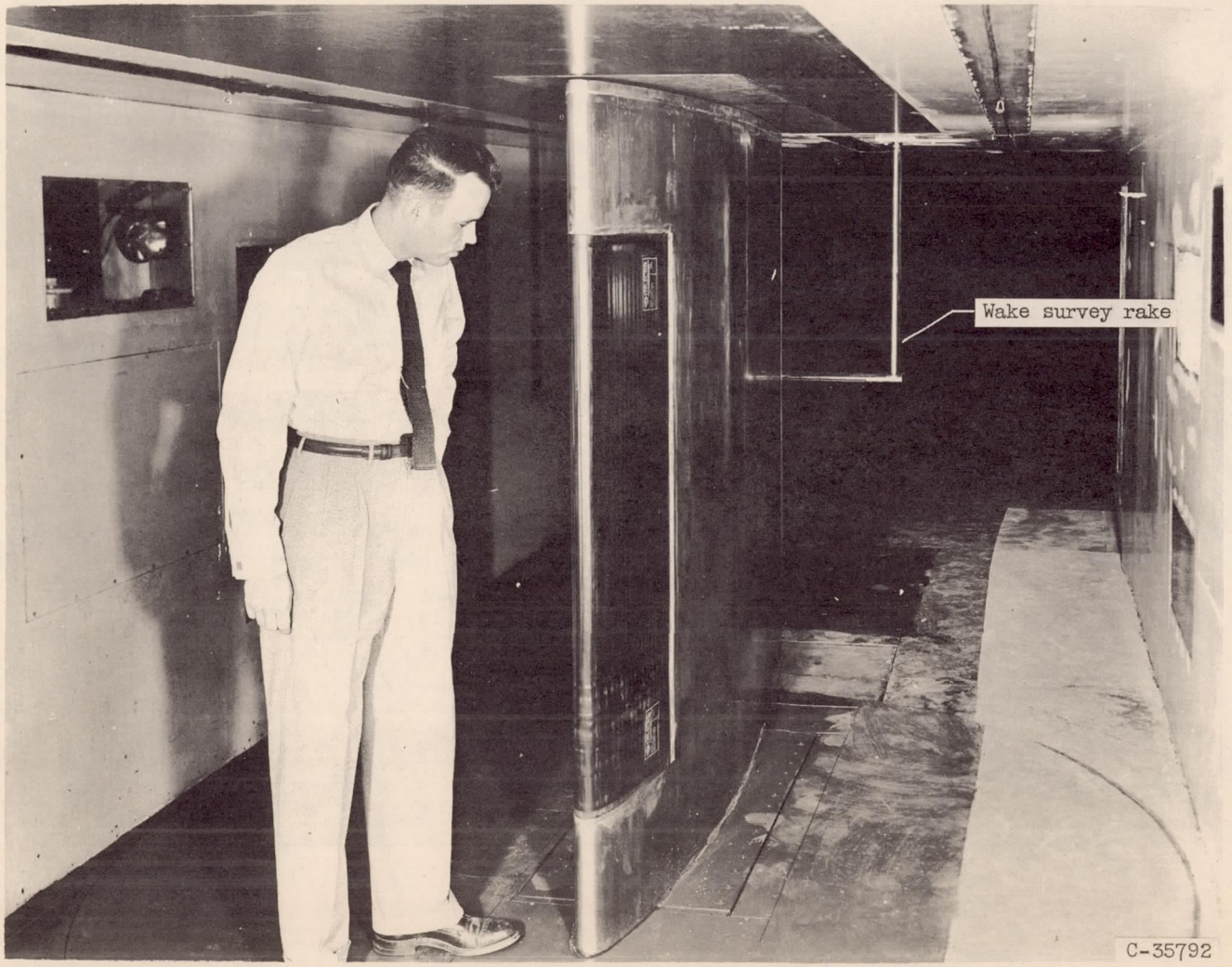

(a) Spanwise-tube de-icer, lower surface.

Figure 1. - Installation of pneumatic de-icer on NACA 0011 airfoil model in 6- by 9-foot icing research tunnel.

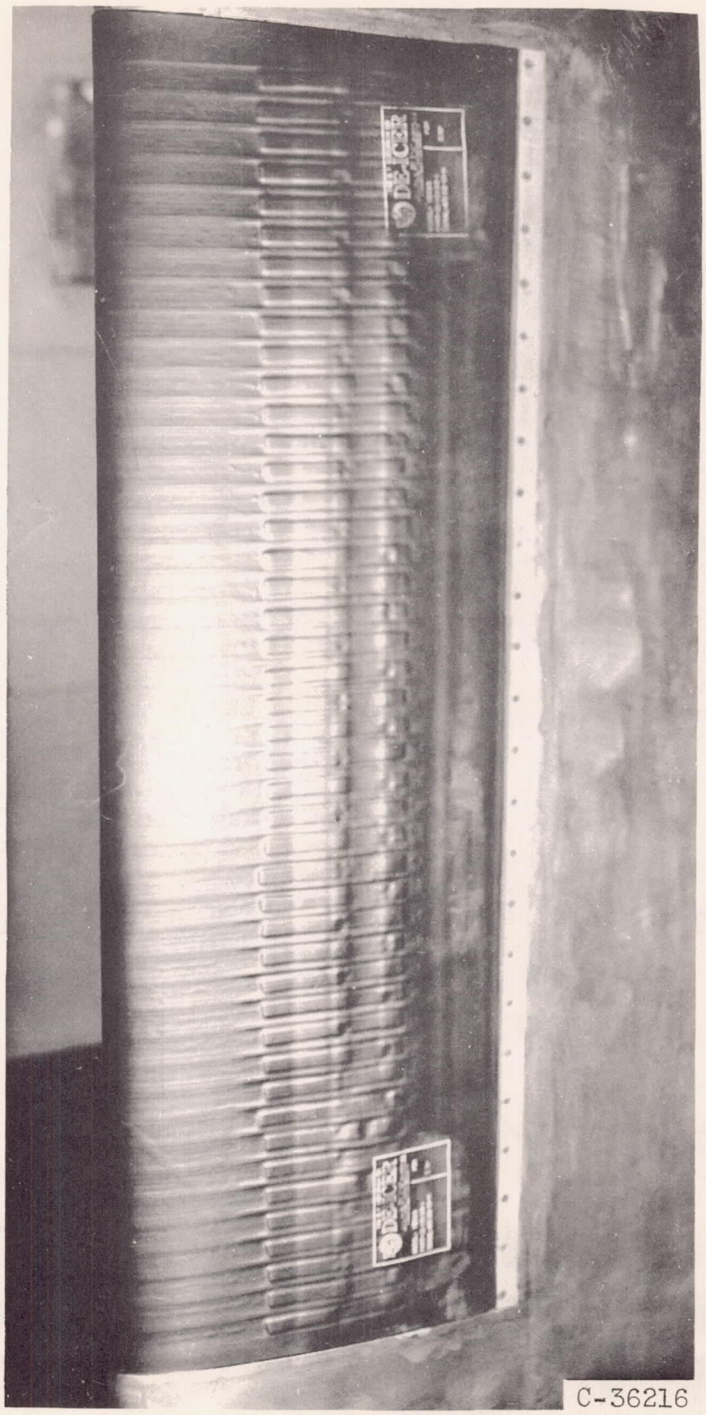

(b) Chordwise-tube de-icer, lower surface.

Figure 1. - Concluded. Installation of pneumatic de-icer on NACA 0011 airfoil model in 6- by 9-foot icing research tunnel.

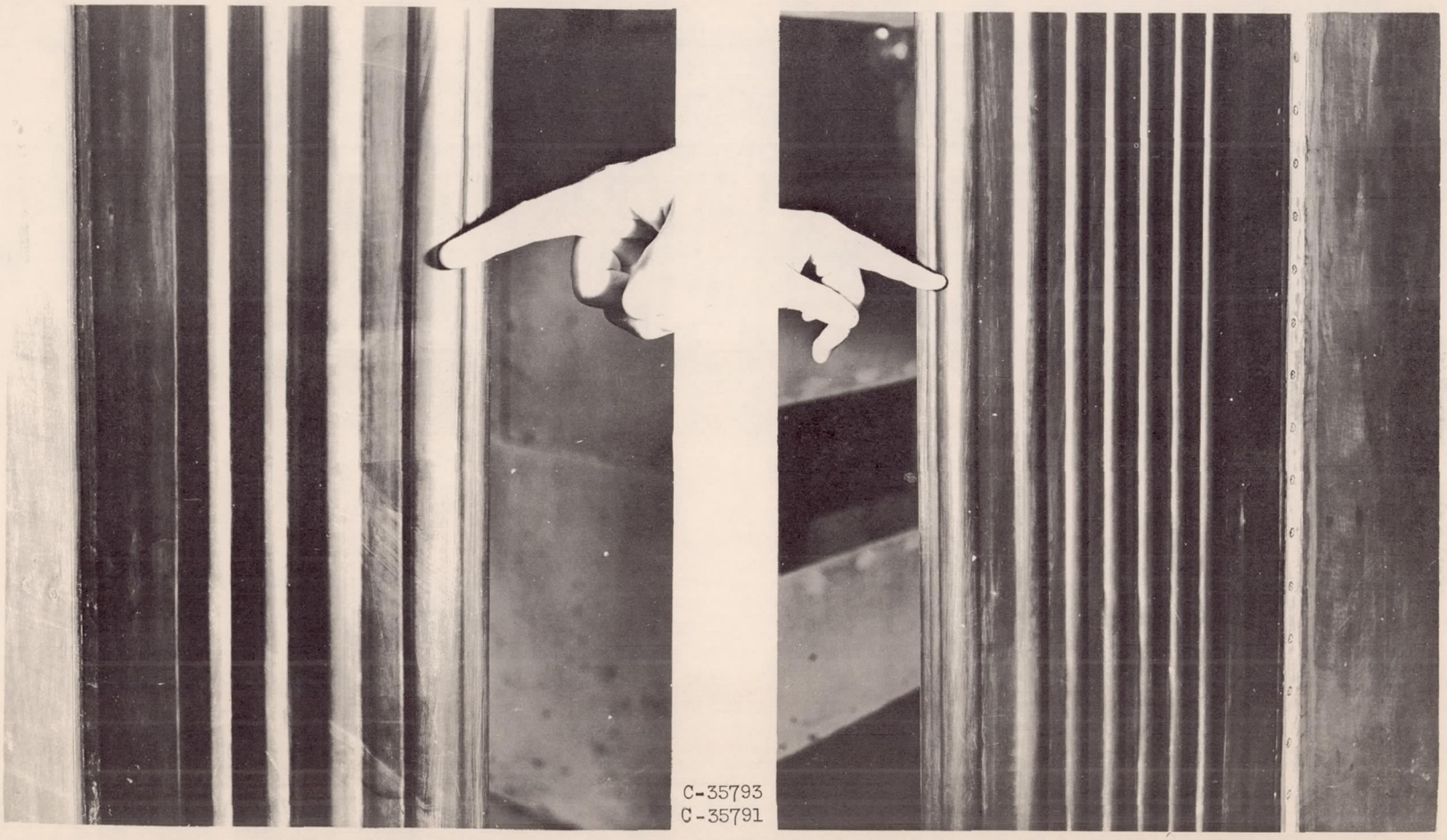

C-35793
C-35791

(a) Spanwise-tube de-icer, upper surface.

(b) Spanwise-tube de-icer, lower surface.

Figure 2. - Photographs of de-icers with A tubes inflated.

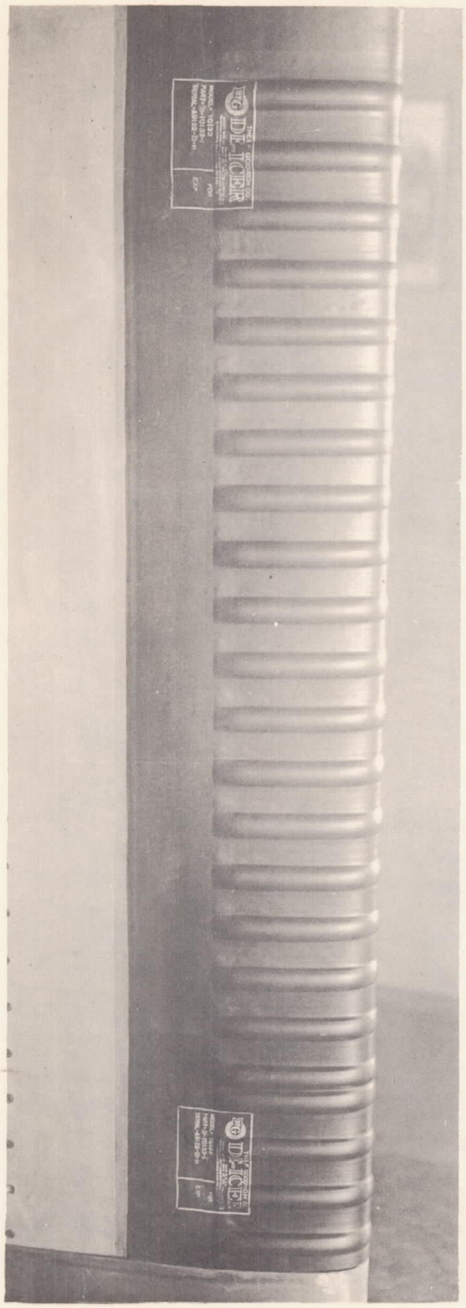

(c) Chordwise-tube de-icer, upper surface.

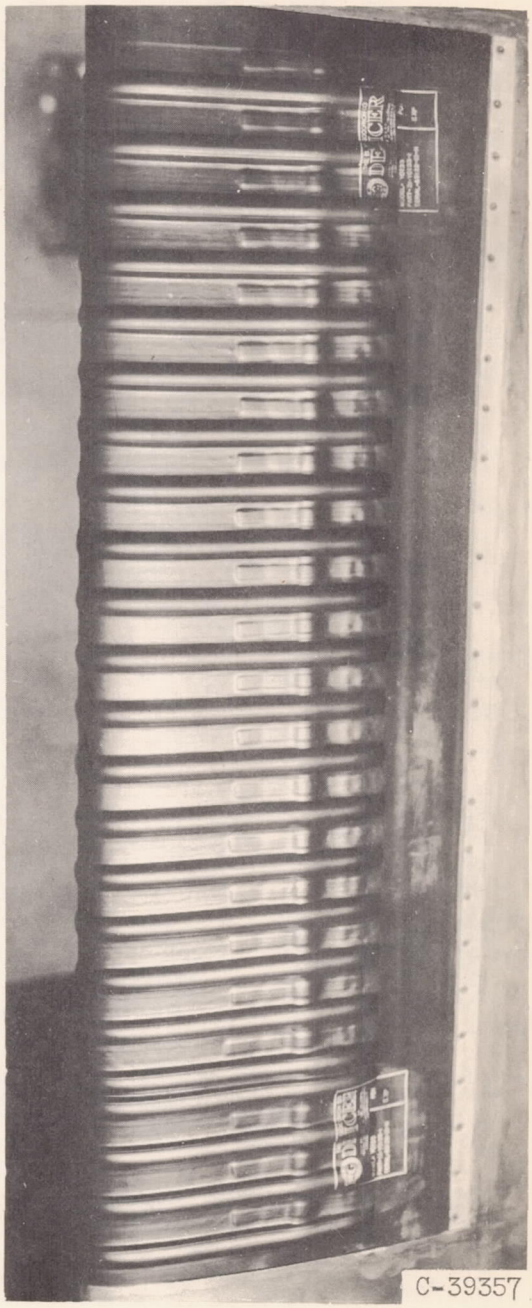

(d) Chordwise-tube de-icer, lower surface.

Figure 2. - Concluded. Photographs of de-icers with A tubes inflated.

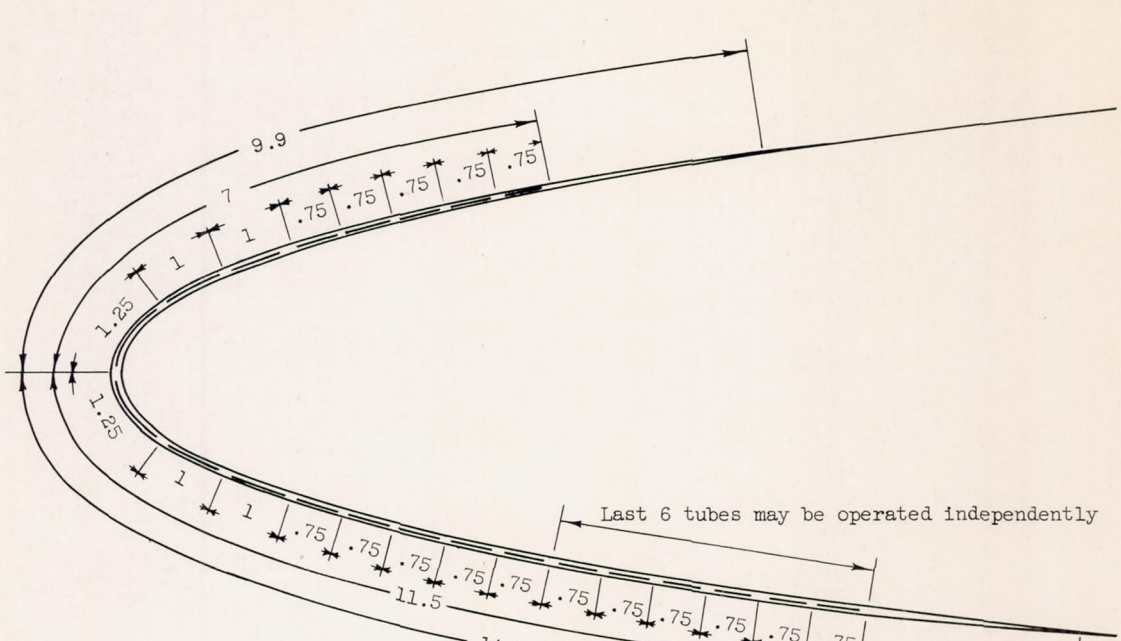

(a) Boot deflated.

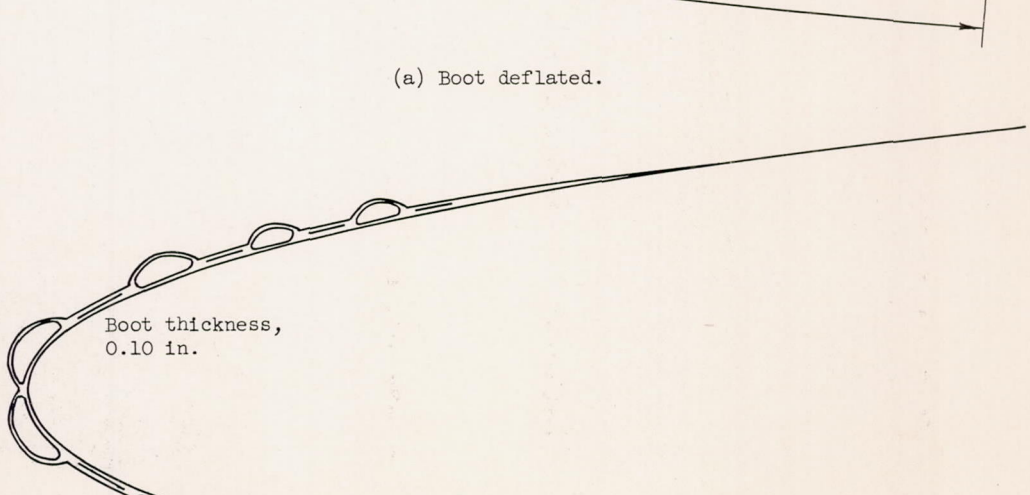

(b) A tubes inflated, B tubes deflated.

Figure 3. - Sketch of spanwise-tube de-icer showing tube locations (dimensions in inches).

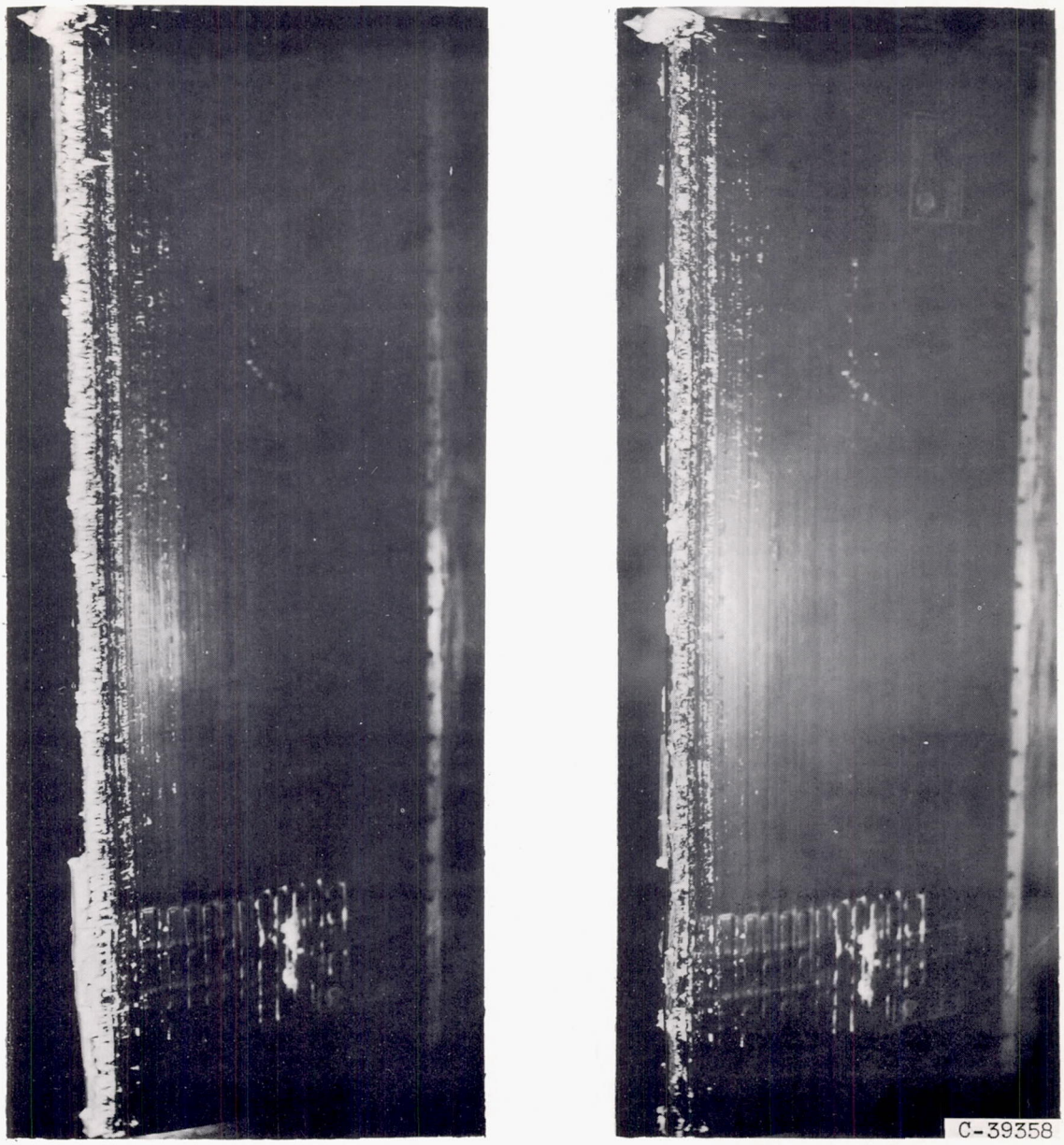

Before ice removal. Section drag coefficient, 0.0082.

After ice removal. Section drag coefficient, 0.0081.

(a) Rime ice. Angle of attack, 0°; airspeed, 175 mph; total air temperature, 10° F; liquid-water content, 0.5 gram per cubic meter; initial section drag coefficient, 0.0072.

Figure 4. - Typical ice formations on airfoil with spanwise-tube de-icer operating. Icing period, 3.9 minutes.

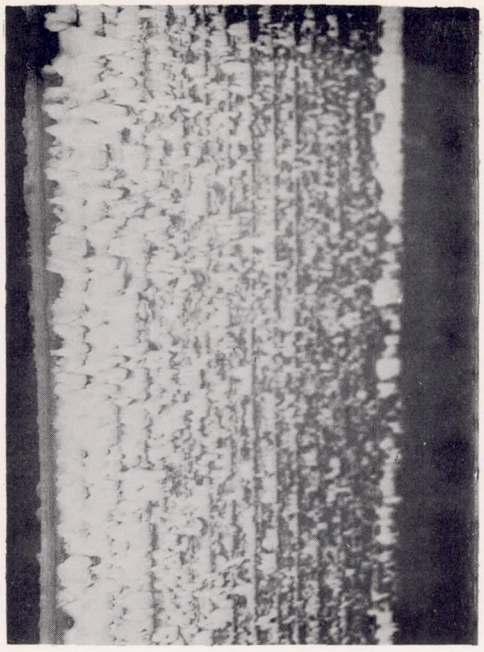

Lower surface before ice removal.
Section drag coefficient, 0.0108;
lift coefficient, 0.196.

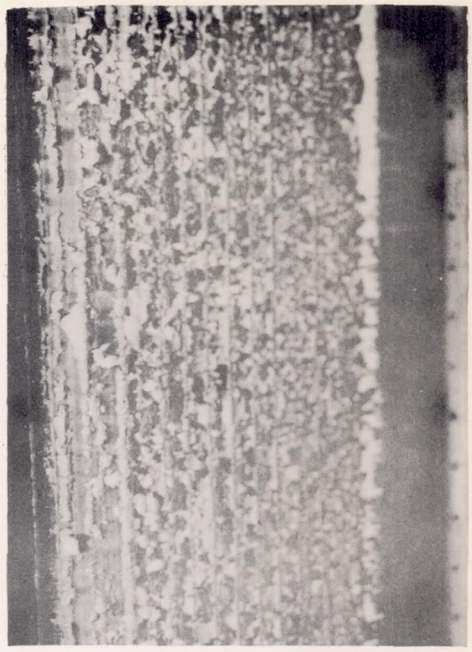

Lower surface after ice removal.
Section drag coefficient, 0.0092;
lift coefficient, 0.198.

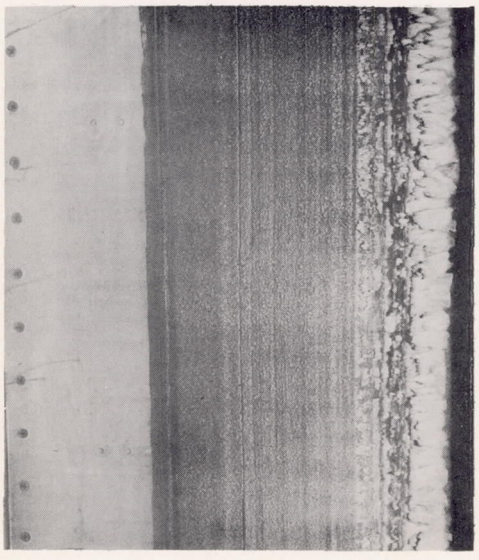

Upper surface before ice removal.

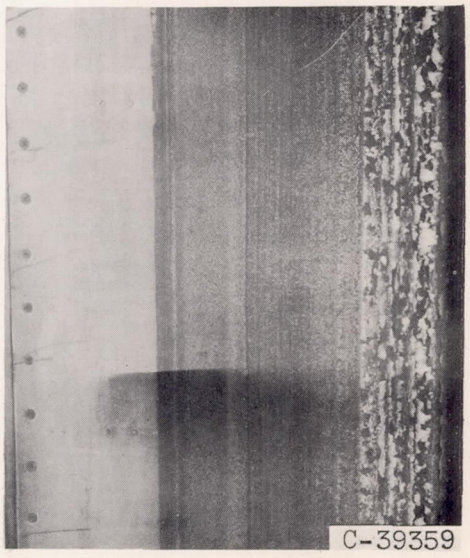

Upper surface after ice removal.

(b) Rime ice. Angle of attack, 2.3°; airspeed, 275 mph; total air temperature, 10° F; liquid-water content, 0.5 gram per cubic meter; initial section drag coefficient, 0.0068; initial lift coefficient, 0.200.

Figure 4. - Continued. Typical ice formations on airfoil with spanwise-tube de-icer operating. Icing period, 3.9 minutes.

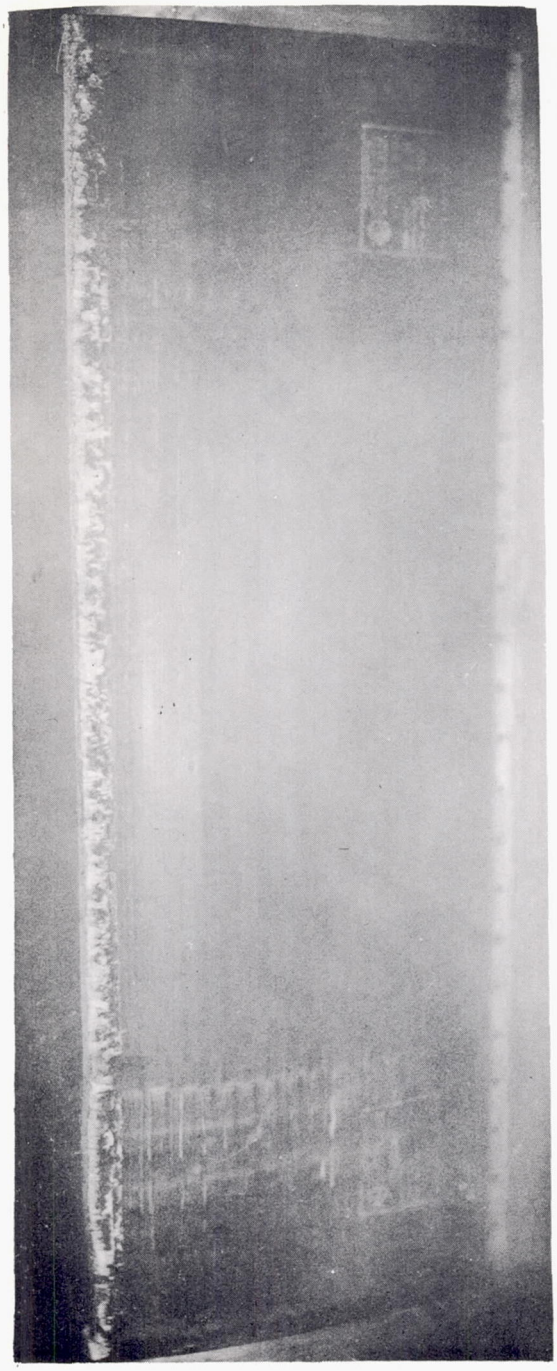

Before ice removal. Section drag coefficient, 0.0086.

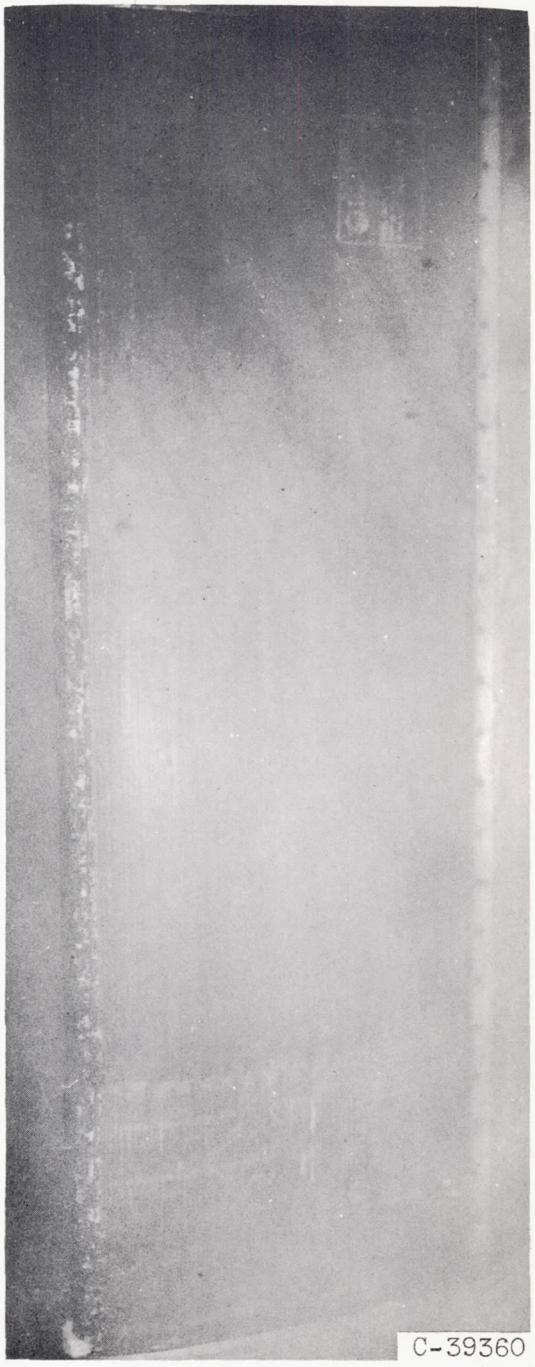

After ice removal. Section drag coefficient, 0.0076.

(c) Glaze ice. Angle of attack, 0°; airspeed, 175 mph; total air temperature, 25° F; liquid-water content, 0.5 gram per cubic meter; initial section drag coefficient, 0.0072.

Figure 4. - Continued. Typical ice formations on airfoil with spanwise-tube de-icer operating. Icing period, 3.9 minutes.

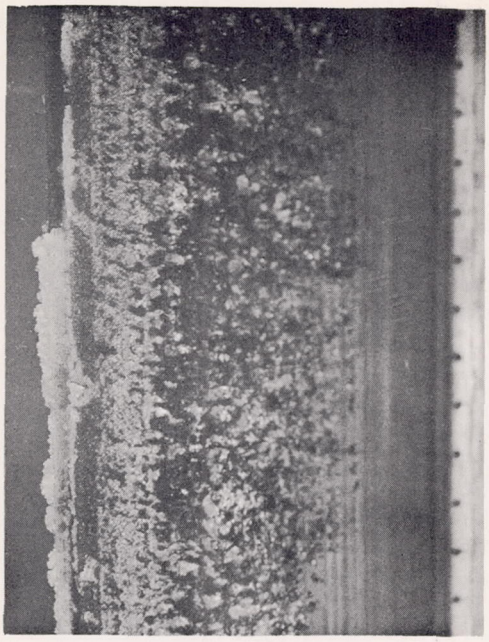

Lower surface before ice removal.
Section drag coefficient, 0.0189;
lift coefficient, 0.556.

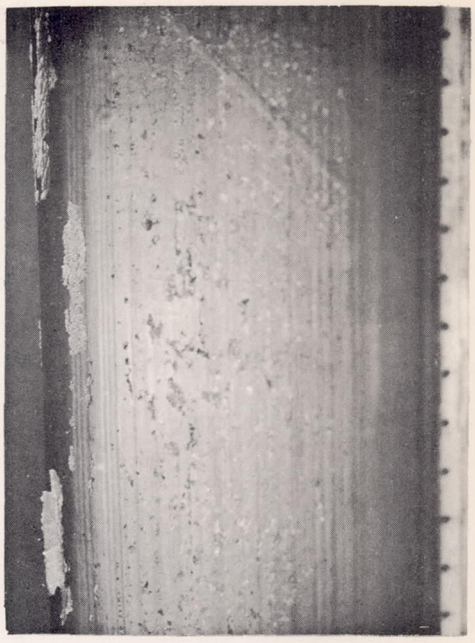

Lower surface after ice removal.
Section drag coefficient, 0.0122;
lift coefficient, 0.578.

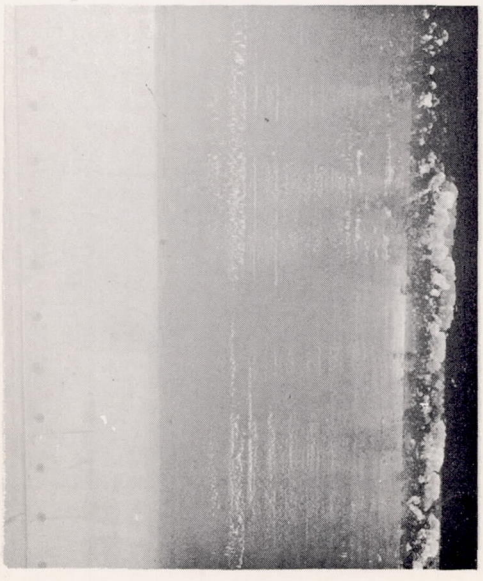

Upper surface before ice removal.

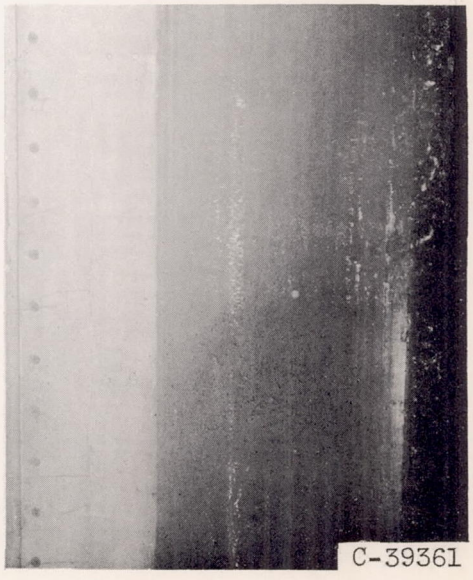

Upper surface after ice removal.

(d) Ridge-type glaze ice. Angle of attack, 7.0°; airspeed, 175 mph; total air temperature, 25° F; liquid-water content, 1.0 gram per cubic meter; initial section drag coefficient, 0.0086; initial lift coefficient, 0.619.

Figure 4. - Concluded. Typical ice formations on airfoil with spanwise-tube de-icer operating. Icing period, 3.9 minutes.

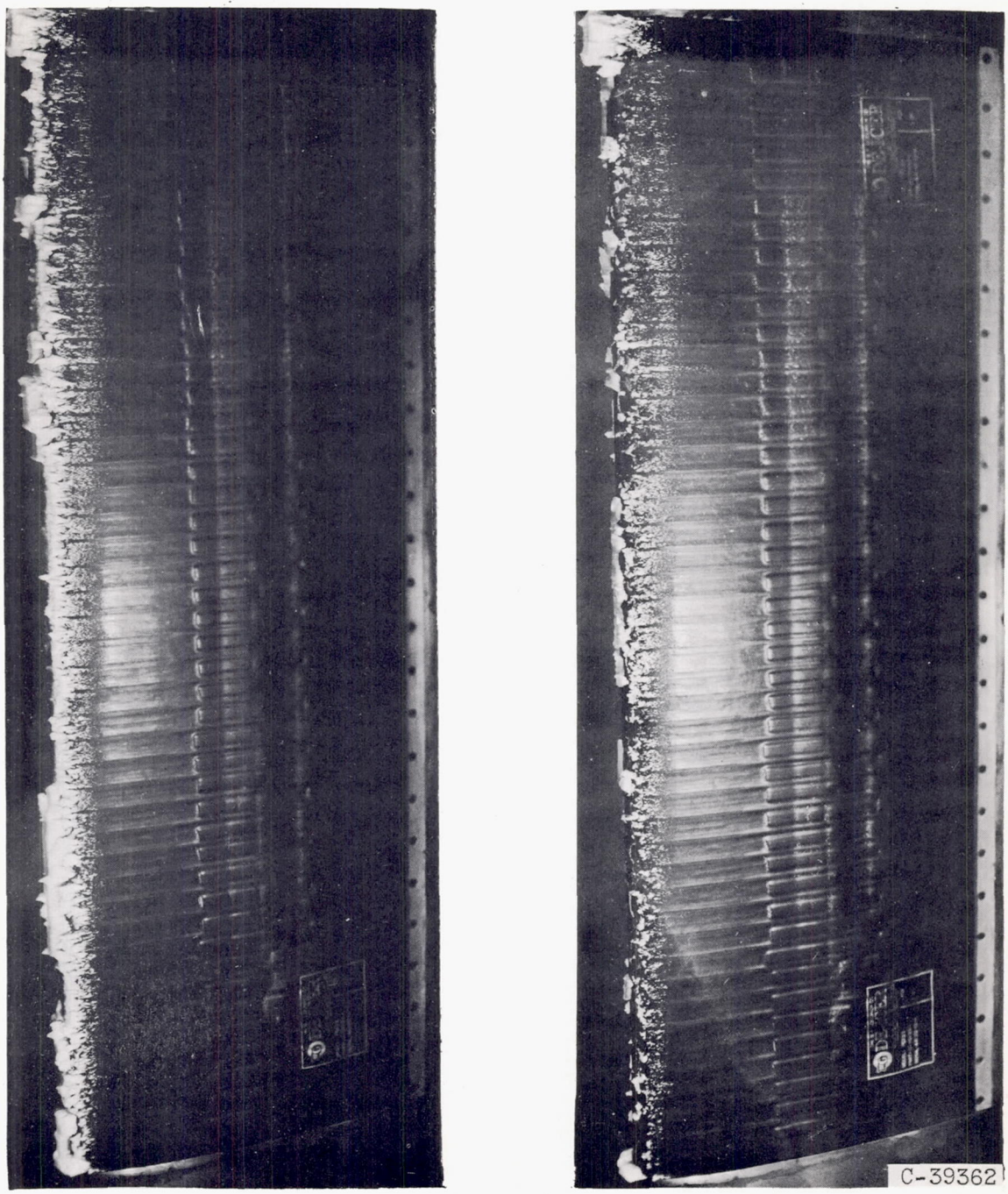

Before ice removal. Section drag coefficient, 0.0085.

After ice removal. Section drag coefficient, 0.0082.

(a) Angle of attack, 0°; initial section drag coefficient, 0.0071.

Figure 5. - Typical rime-ice formations on airfoil with chordwise-tube de-icer operating. Airspeed, 175 mph; total air temperature, 10° F; liquid-water content, 0.5 gram per cubic meter; icing period, 3.9 minutes.

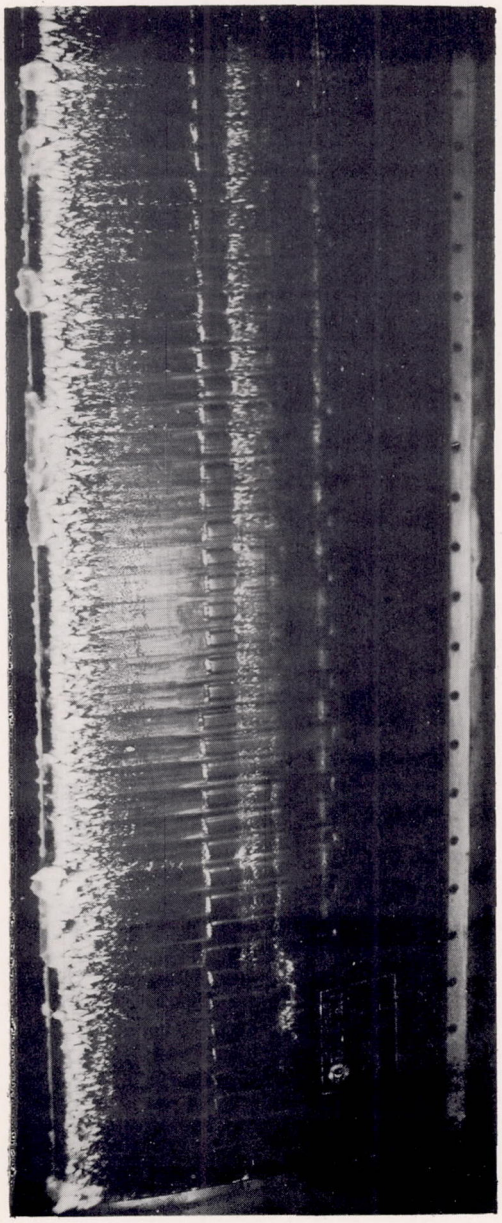

Lower surface before ice removal.
Section drag coefficient, 0.0087;
lift coefficient, 0.186.

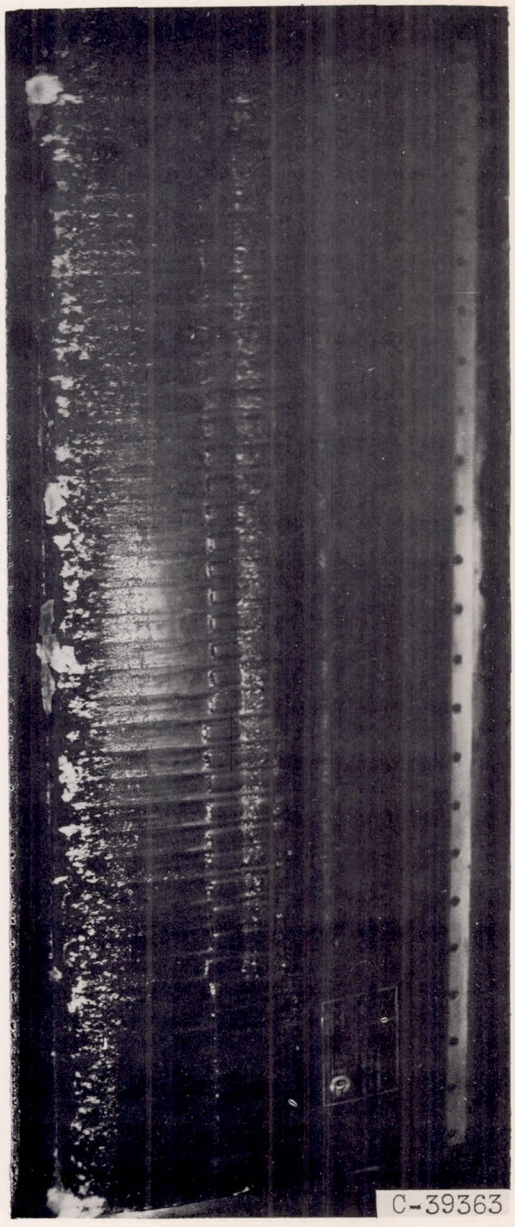

Lower surface after ice removal.
Section drag coefficient, 0.0083;
lift coefficient, 0.188.

(b) Angle of attack, 2.3°; initial section drag coefficient, 0.0074; initial lift coefficient, 0.196.

Figure 5. - Concluded. Typical rime-ice formations on airfoil with chordwise-tube de-icer operating. Airspeed, 175 mph; total air temperature, 10° F; liquid-water content, 0.5 gram per cubic meter; icing period 3.9 minutes.

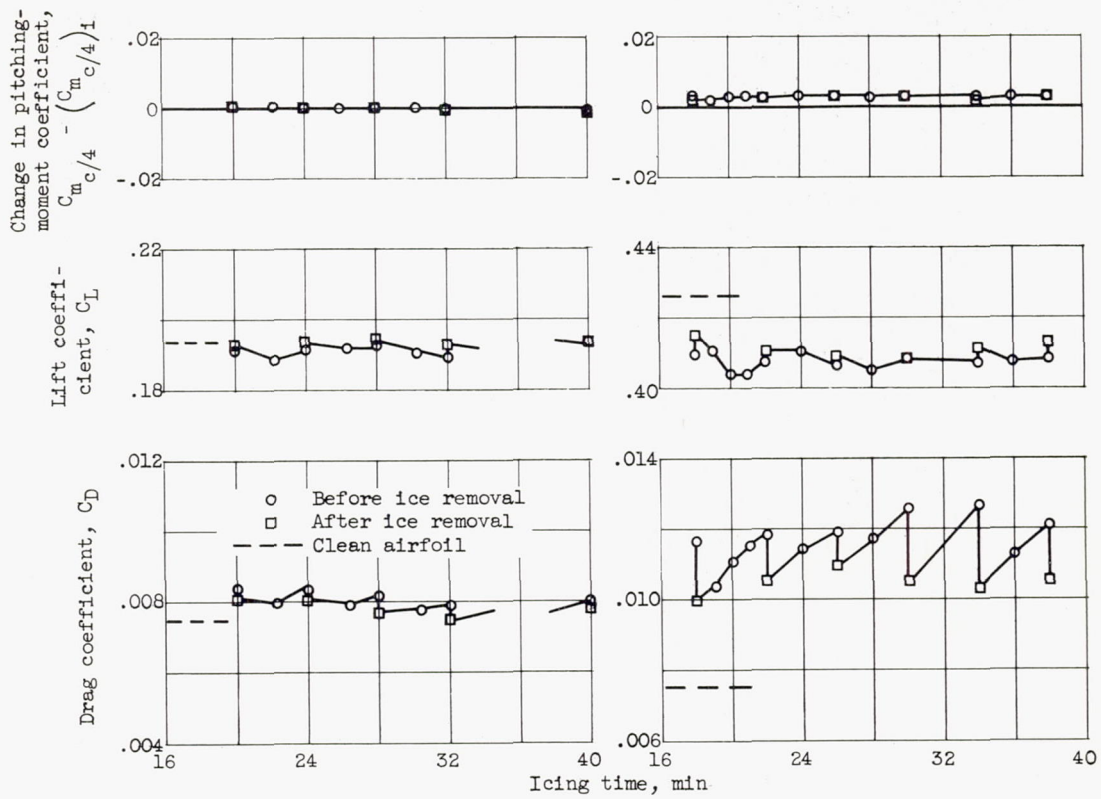

(a) Angle of attack, 2.3°; airspeed, 175 mph; maximum droplet size, 23 microns; ice-accretion rate, 0.9 pound per hour per foot span.

(b) Angle of attack, 4.6°; airspeed, 275 mph; maximum droplet size, 37 microns; ice-accretion rate, 2.8 pounds per hour per foot span.

Figure 6. - Typical variation of airfoil section drag, lift, and pitching-moment coefficients in rime-icing conditions with spanwise-tube de-icer operating. Total air temperature, 10° F; liquid-water content, 0.5 gram per cubic meter; icing period, 3.9 minutes.

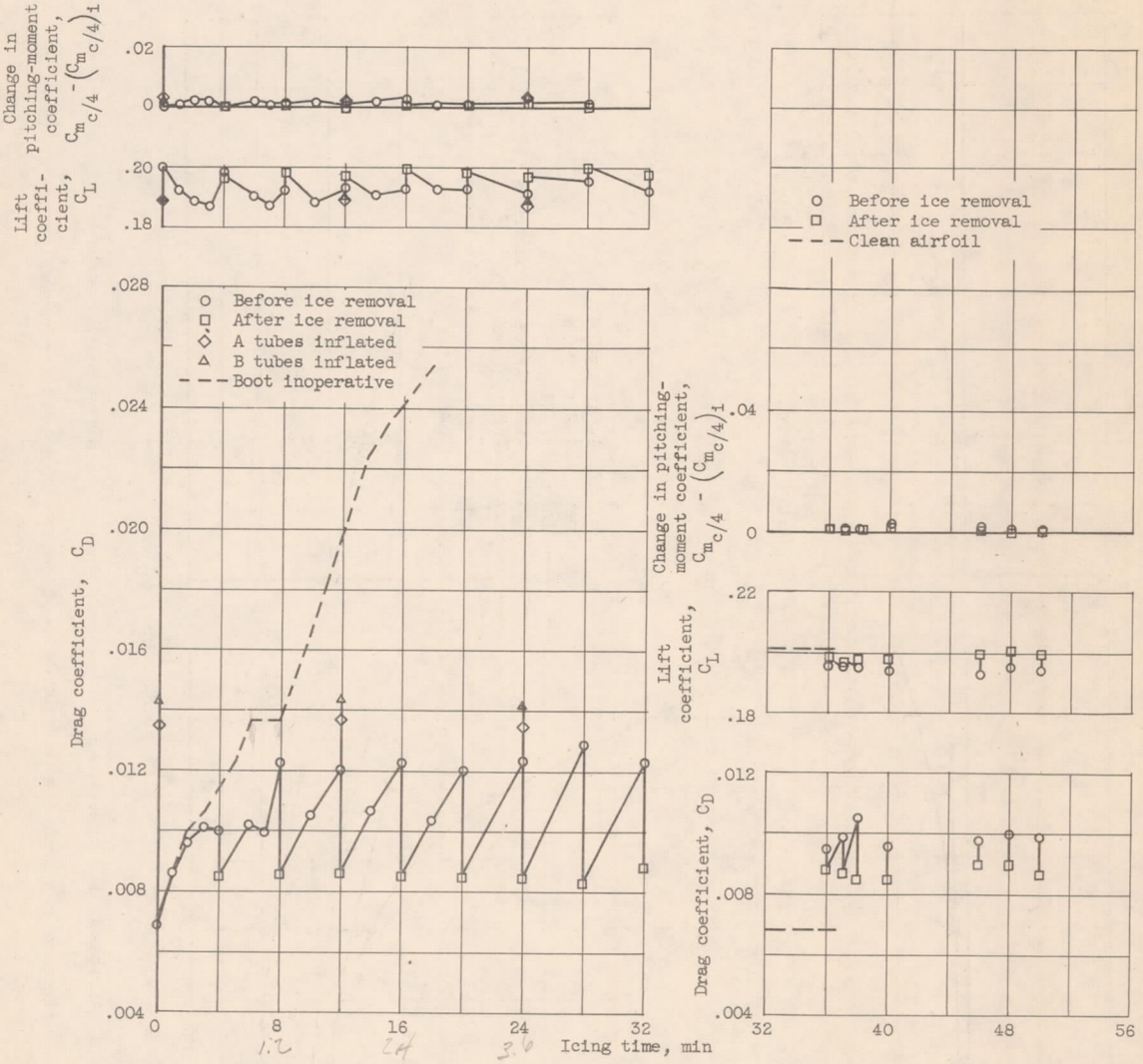

(a) Icing period, 3.9 minutes.

(b) Icing period, 0.9 minute.

Figure 7. - Typical variation of airfoil section drag, lift, and pitching-moment coefficients in glaze-icing conditions with spanwise-tube de-icer operating. Angle of attack, 2.3°; airspeed, 275 mph; total air temperature, 25° F; liquid-water content, 0.5 gram per cubic meter; maximum droplet size, 37 microns; ice-accretion rate, 2.7 pounds per hour per foot span.

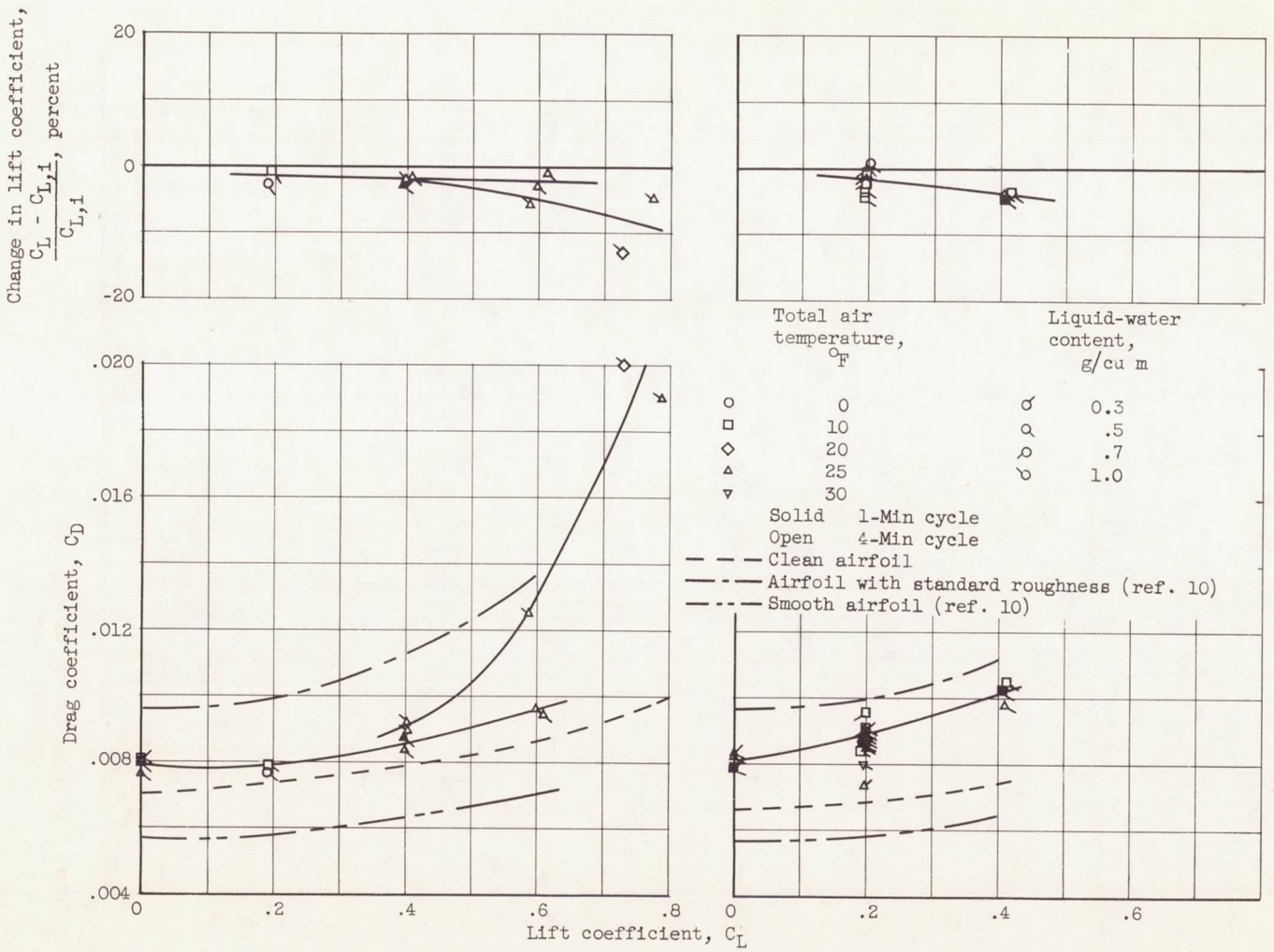

(a) Airspeed, 175 mph.

(b) Airspeed, 275 mph.

Figure 8. - Effect of residual ice on airfoil section drag and lift for spanwise-tube de-icer.

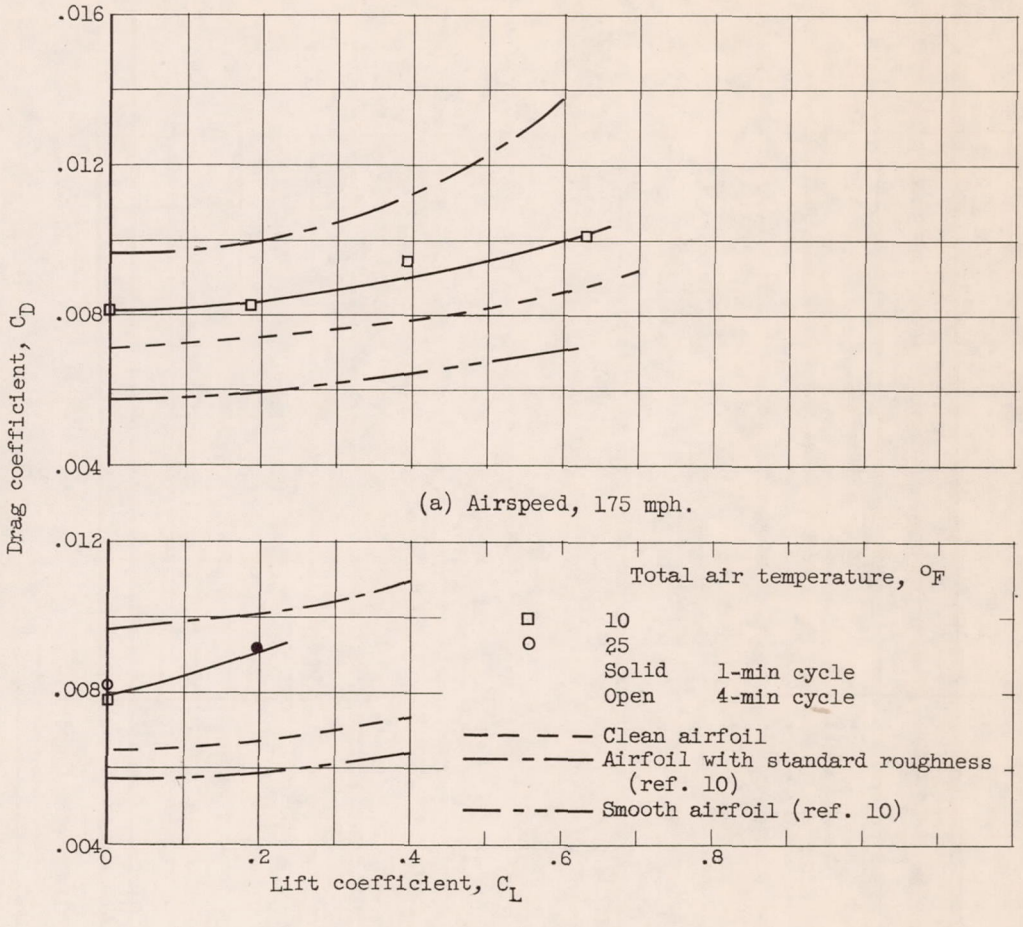

Figure 9. - Effect of residual ice on airfoil drag for chordwise-tube de-icer. Liquid-water content, 0.5 gram per cubic meter.

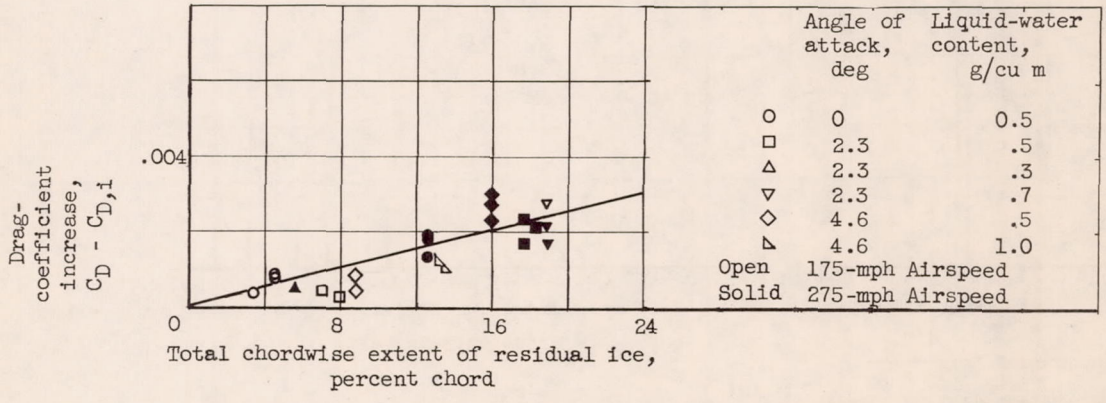

Figure 10. - Drag increase as function of total chordwise extent of residual ice. Icing periods, 0.9 to 3.9 minutes; total air temperature, 0° to 25° F; spanwise-tube de-icer.

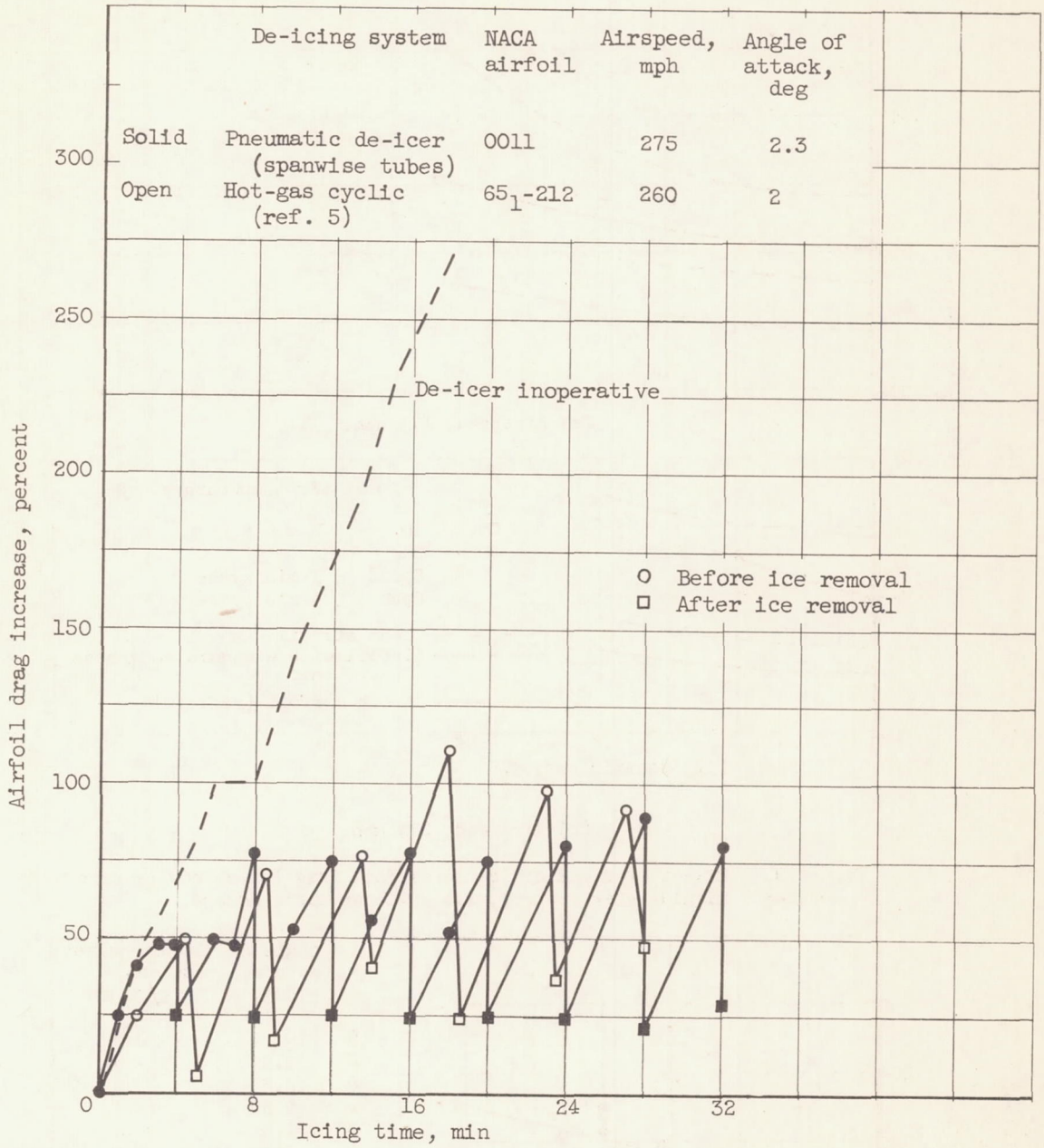

Figure 11. - Comparison of airfoil drag with thermal and pneumatic de-icing systems in heavy glaze-icing conditions. Total air temperature, 25° F.

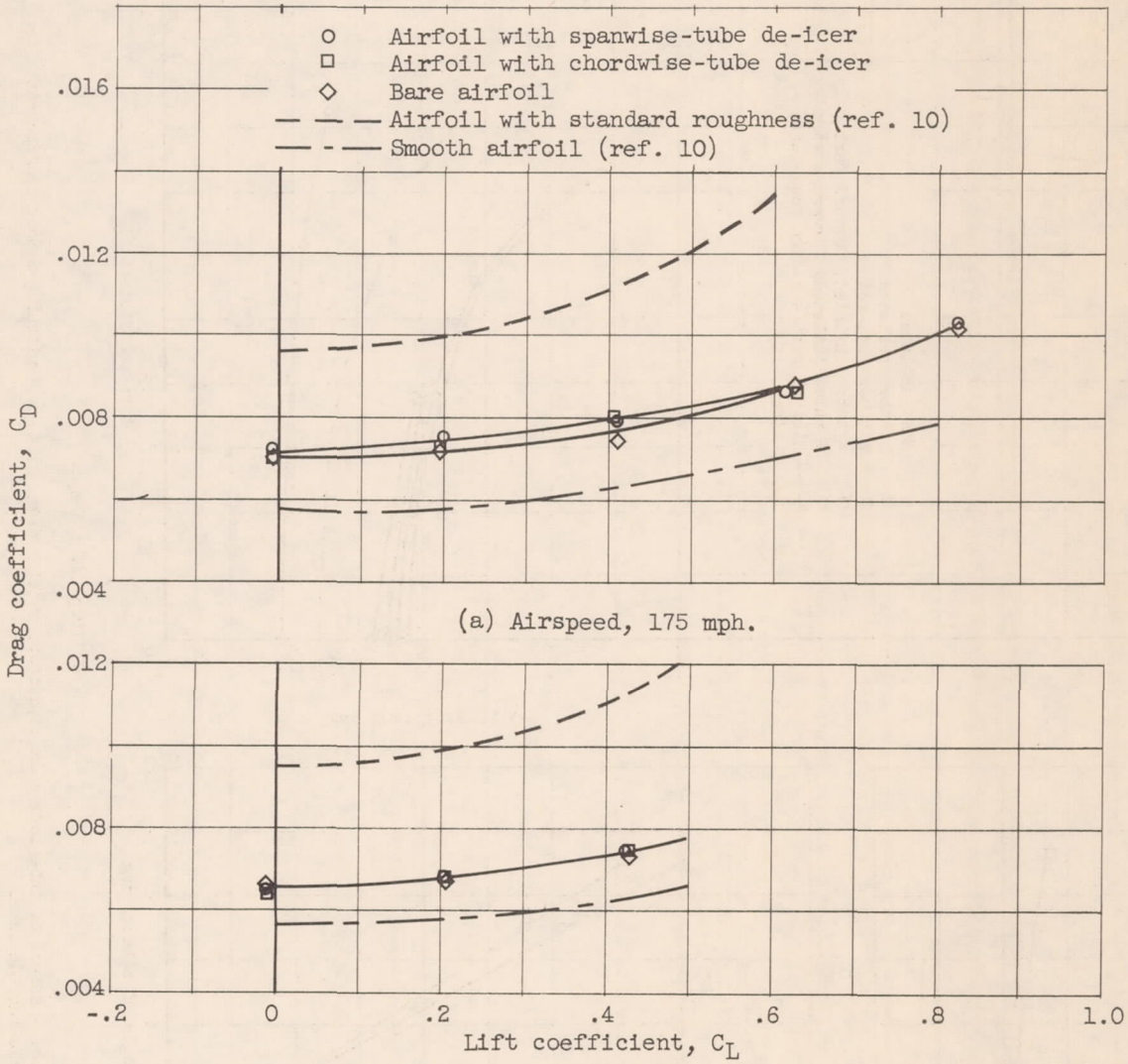

Figure 12. - Comparison of bare-airfoil drag with drag of airfoil having chordwise- and spanwise-tube de-icers.

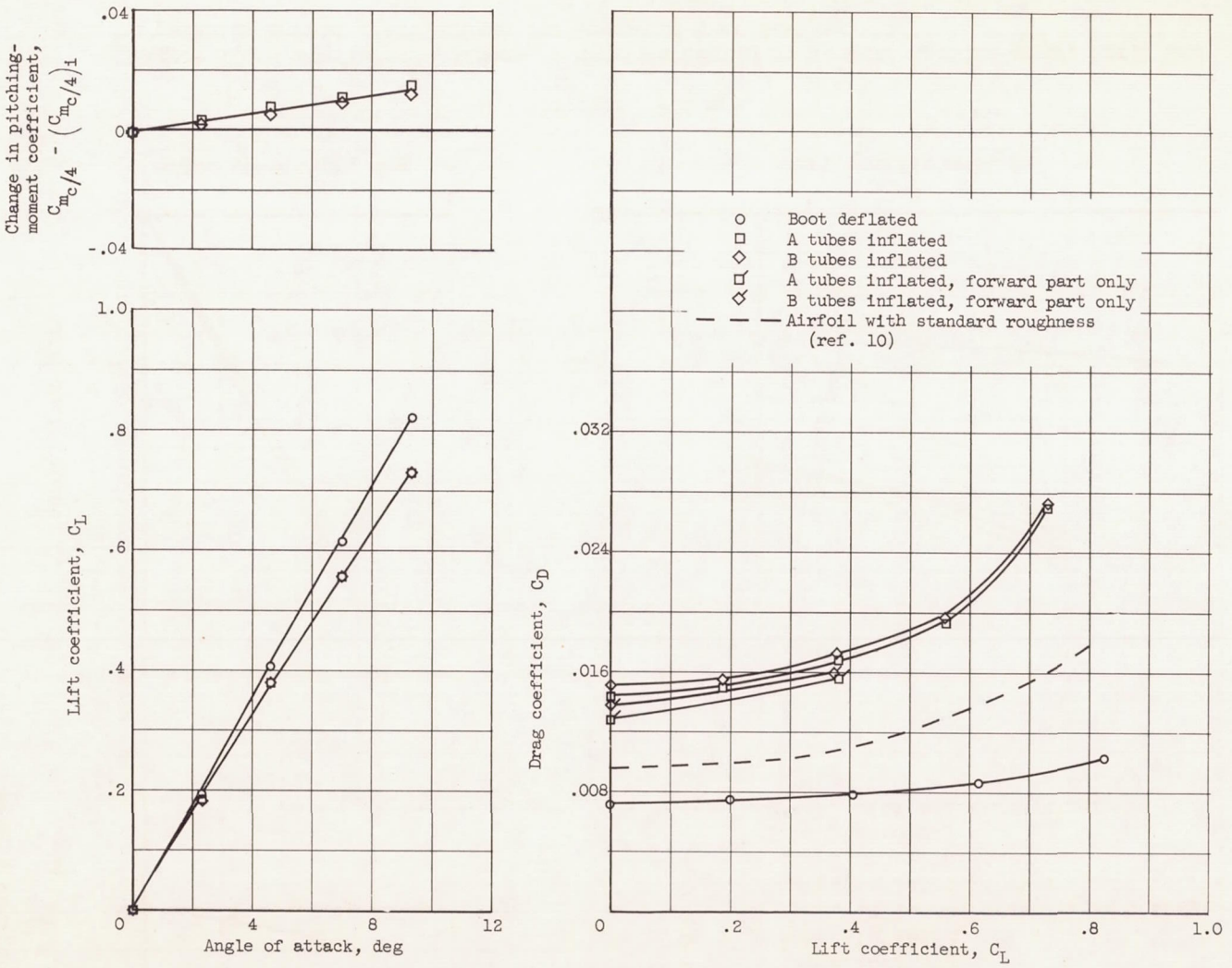

(a) Airspeed, 175 mph.

Figure 13. - Effect of tube inflation on airfoil section drag, lift, and pitching-moment coefficients for spanwise-tube de-icer.

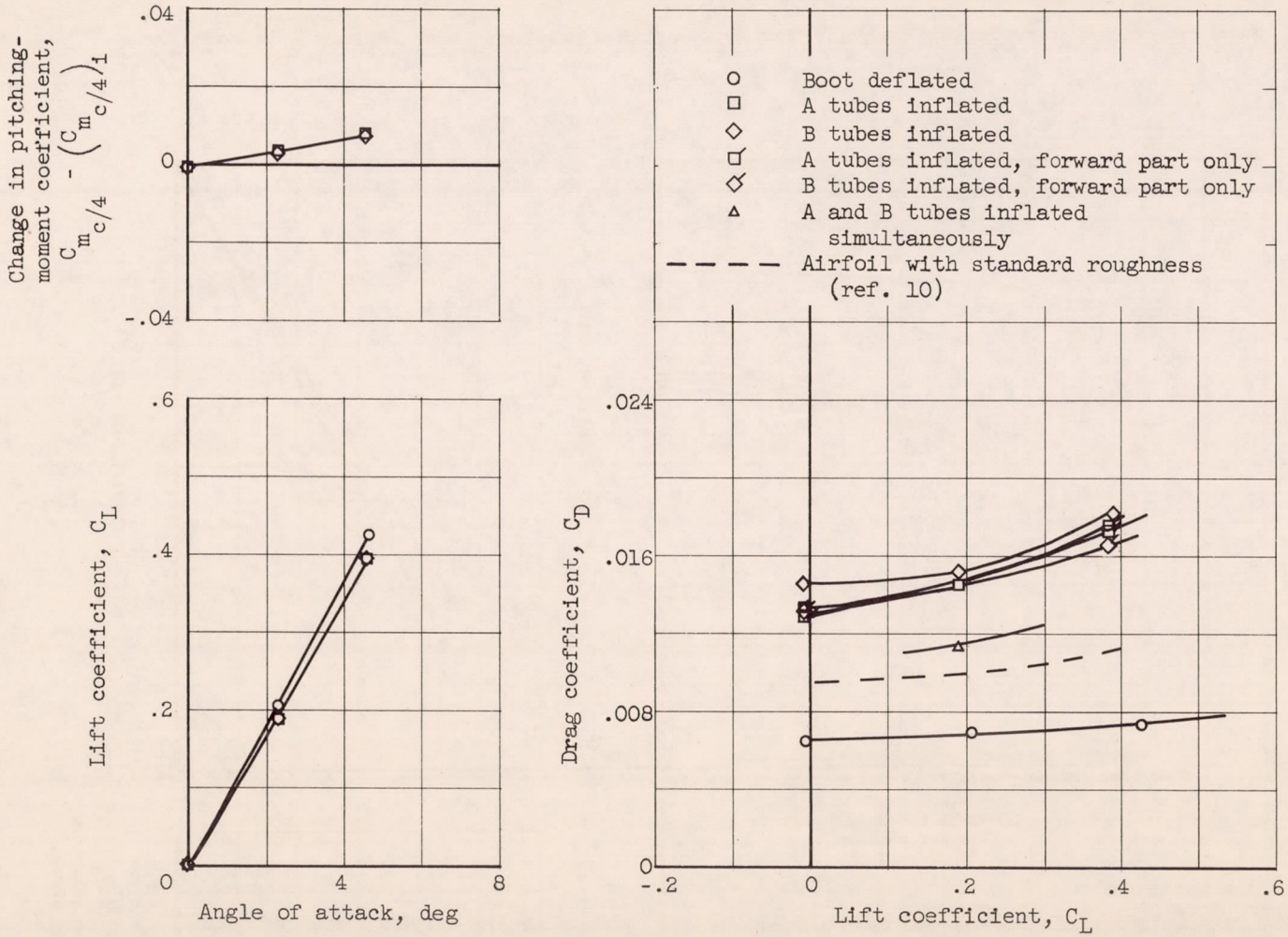

(b) Airspeed, 275 mph.

Figure 13. - Concluded. Effect of tube inflation on airfoil section drag, lift, and pitching-moment coefficients for spanwise-tube de-icer.

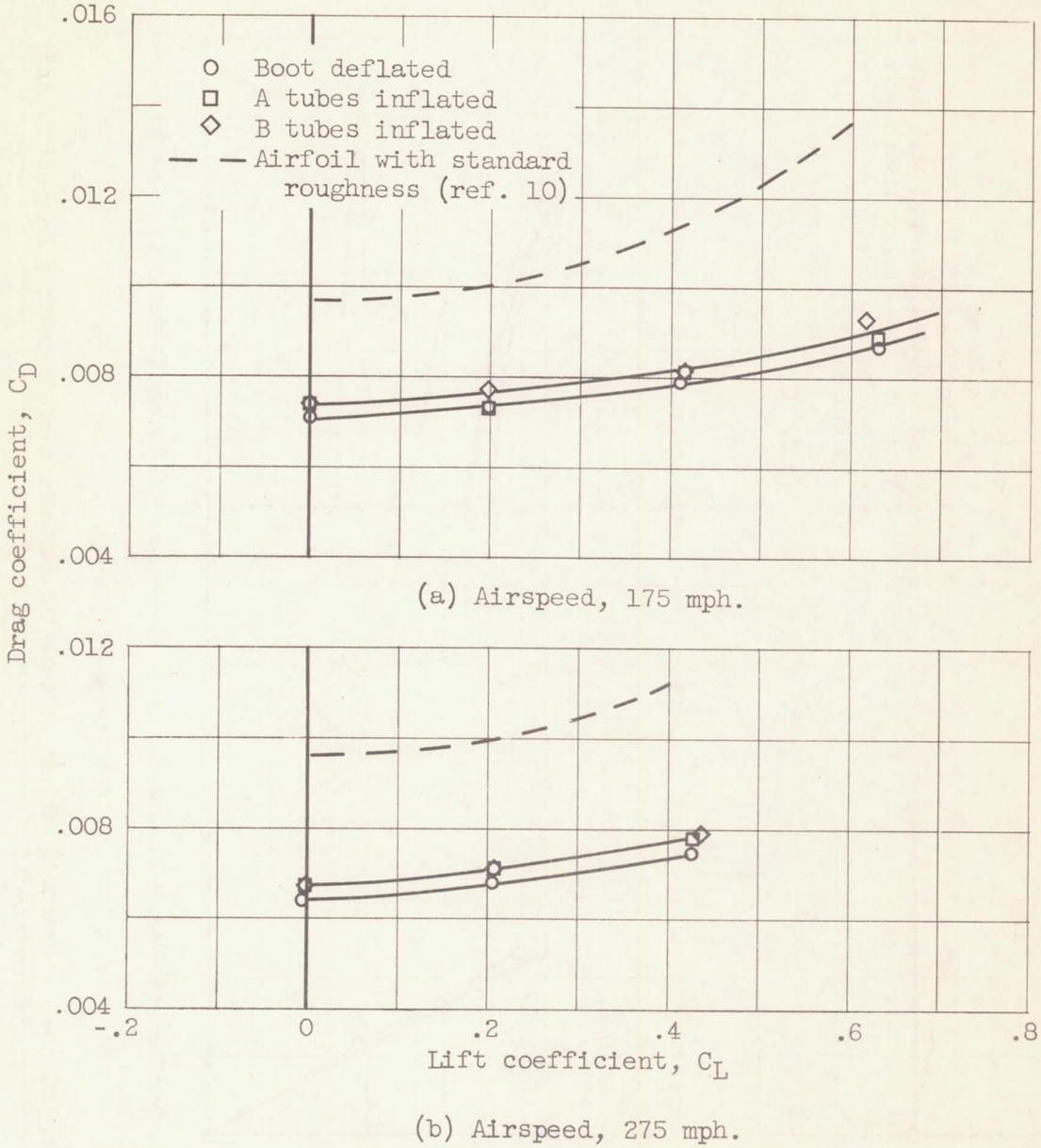

Figure 14. - Effect of tube inflation on airfoil section drag coefficient for chordwise-tube de-icer.

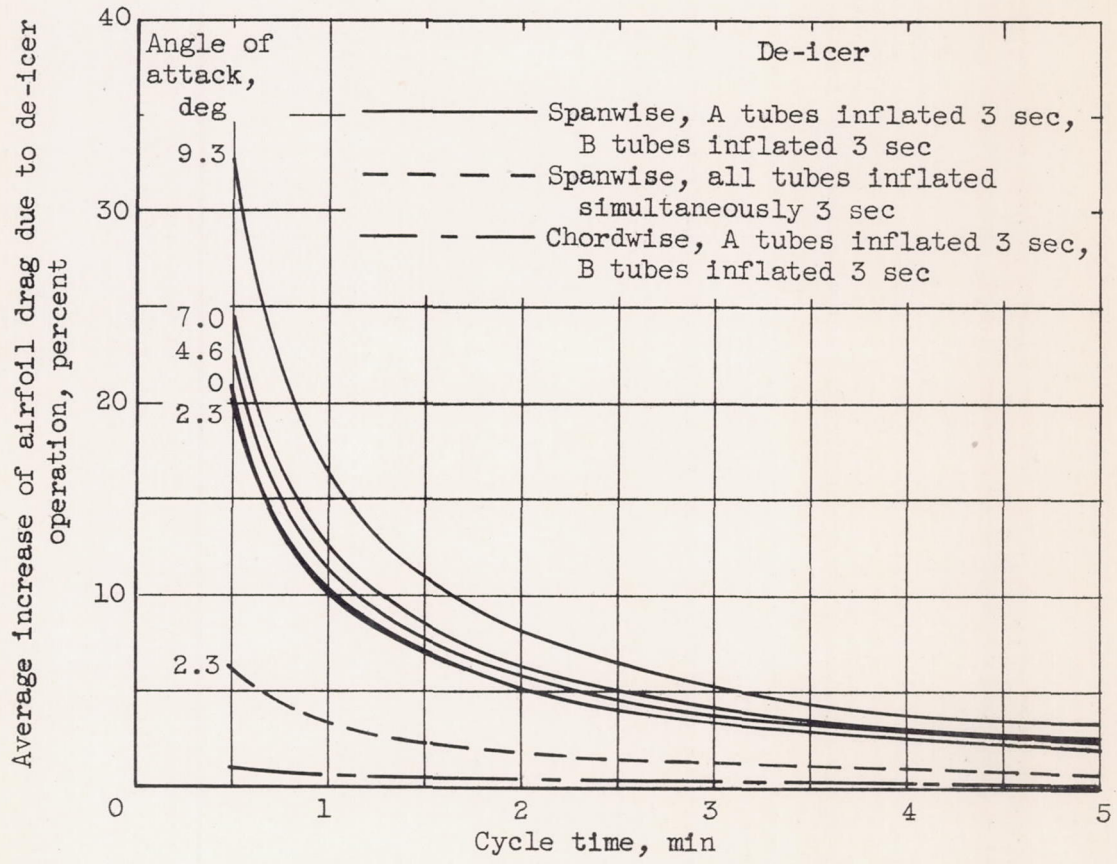

Figure 15. - Average airfoil drag increase due to de-icer operation in dry air as function of cycle time.

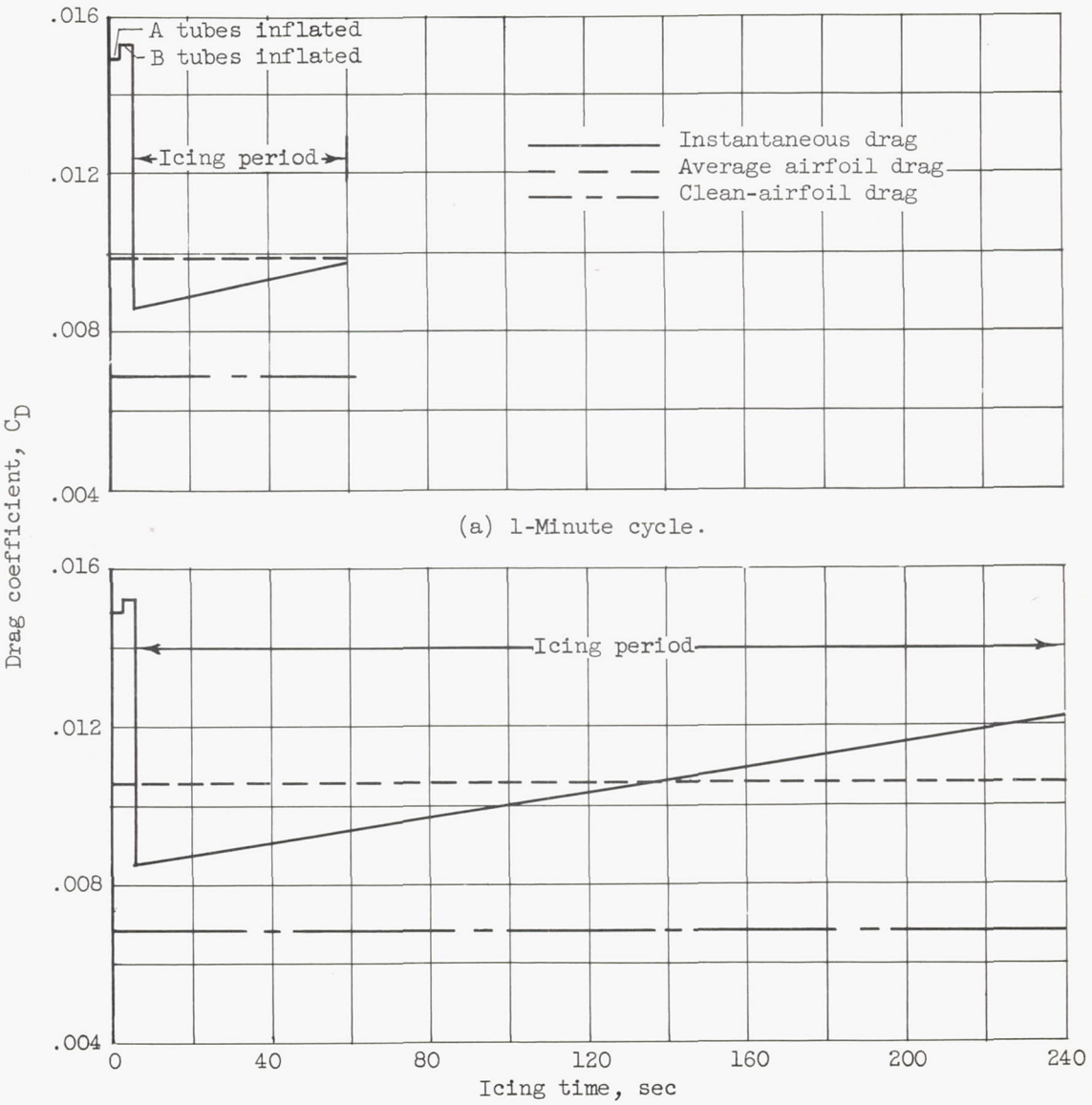

Figure 16. - Typical determination of average airfoil drag in icing with spanwise-tube de-icer operating. Airspeed, 275 mph; angle of attack, 2.3°; total air temperature, 25° F; liquid-water content, 0.5 gram per cubic meter.

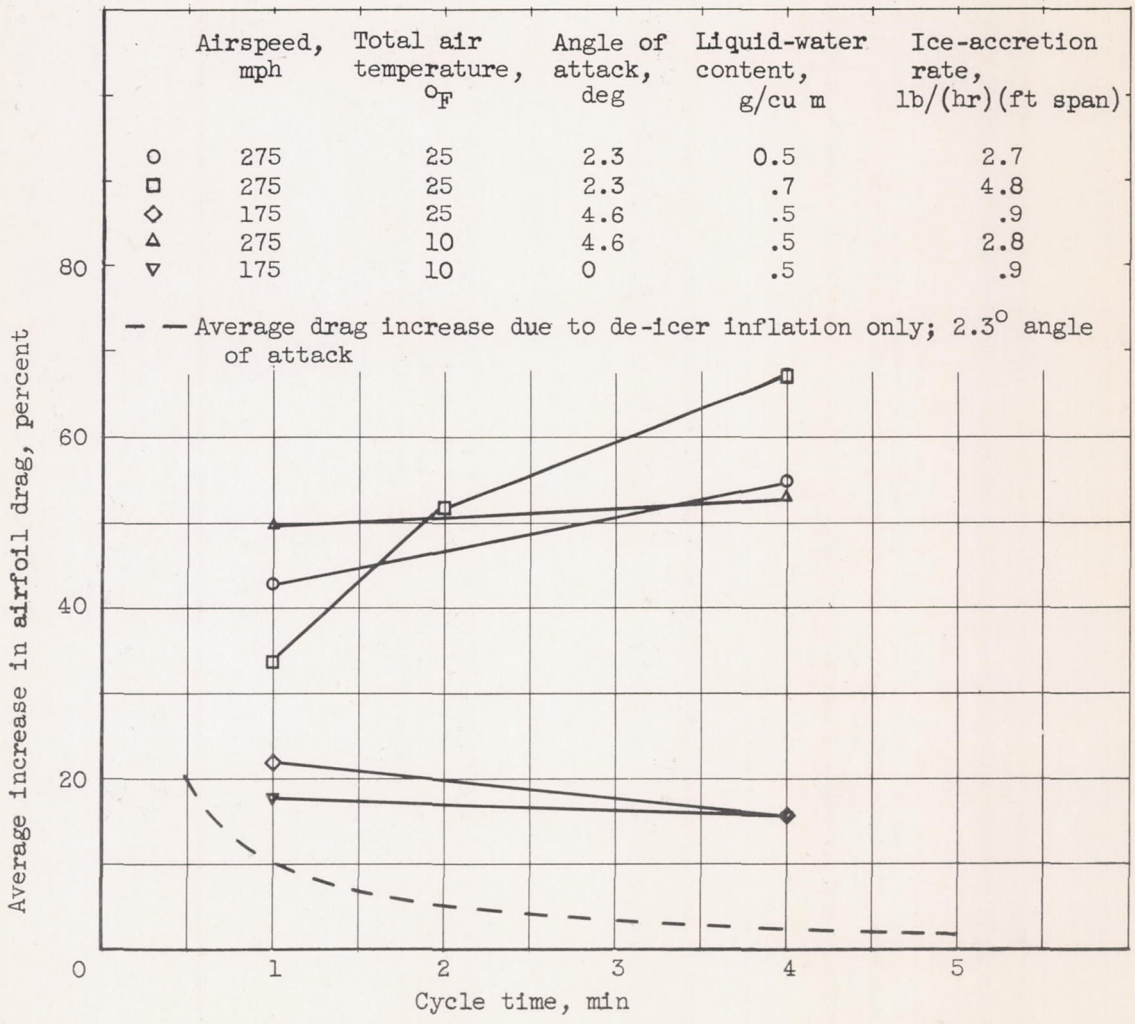

Figure 17. - Average airfoil drag increase in icing with spanwise de-icer operating as function of cycle time.

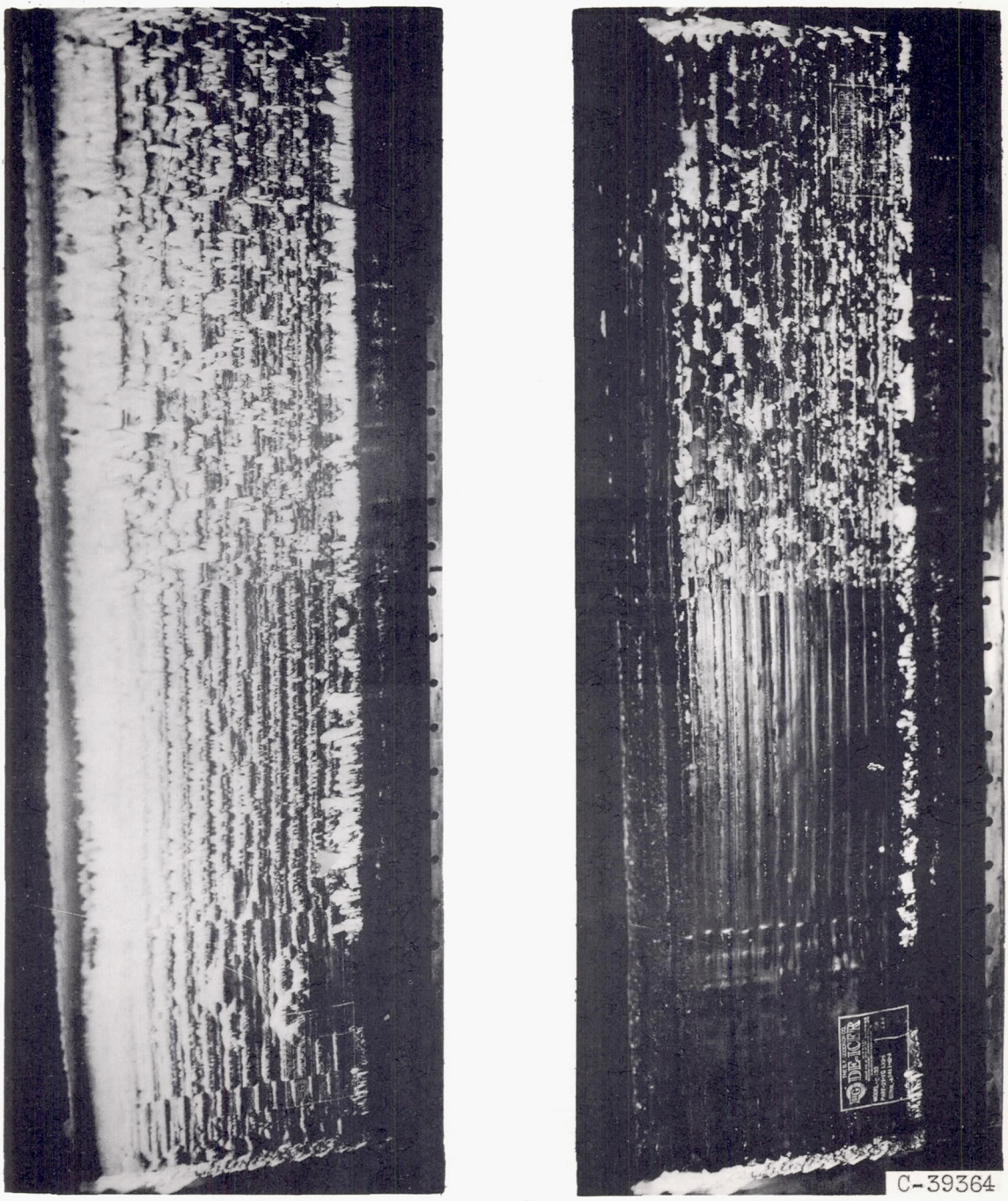

Lower surface before ice removal.

Lower surface after ice removal.

Figure 18. - Effect of coating to reduce ice adhesion on ice-removal characteristics of spanwise-tube de-icers. Lower half of boot coated. Angle of attack, 4.6°; airspeed, 275 mph; total air temperature, 10° F; icing period, 3.9 minutes.

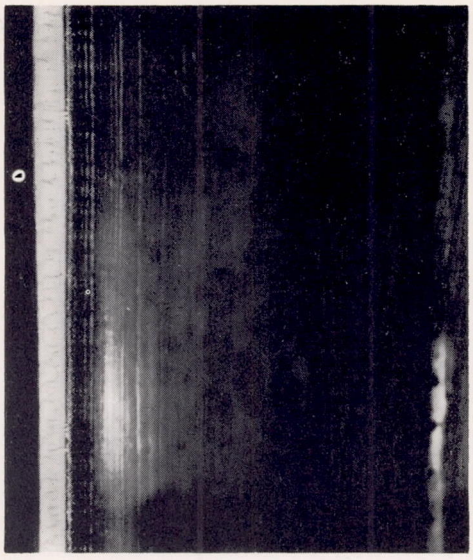

(a) Angle of attack, 0°; airspeed, 175 mph; icing time, 11 minutes; ice accumulation, 0.16 pound per foot span; section drag coefficient, 0.0080; initial section drag coefficient, 0.0072.

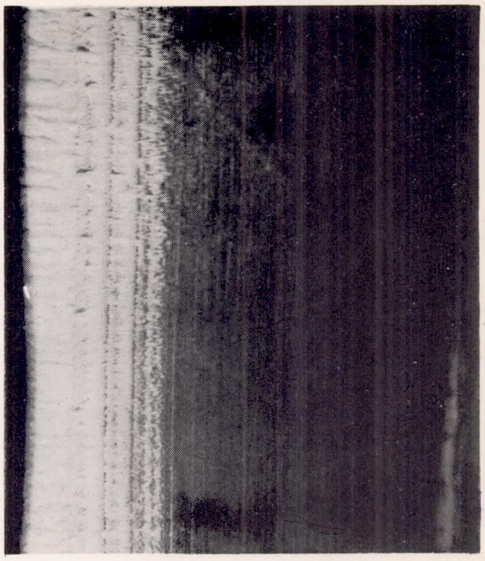

(b) Angle of attack, 0°; airspeed, 275 mph; icing time, 12 minutes; ice accumulation, 0.52 pound per foot span; section drag coefficient, 0.0090; initial section drag coefficient, 0.0066.

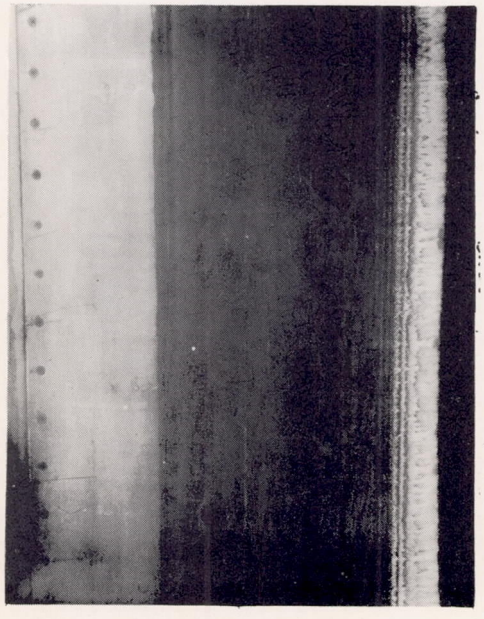

Upper surface

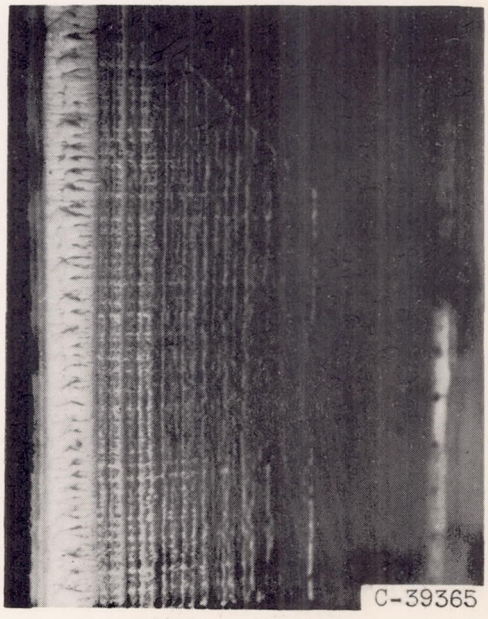

Lower surface

(c) Angle of attack, 2.3°; airspeed, 175 mph; icing time, 15 minutes; ice accumulation, 0.22 pound per foot span; section drag coefficient, 0.0089; initial section drag coefficient, 0.0075; lift coefficient, 0.192; initial lift coefficient, 0.194.

Figure 19. - Typical rime-ice formations on airfoil. Total air temperature, 10° F; liquid-water content, 0.5 gram per cubic meter.

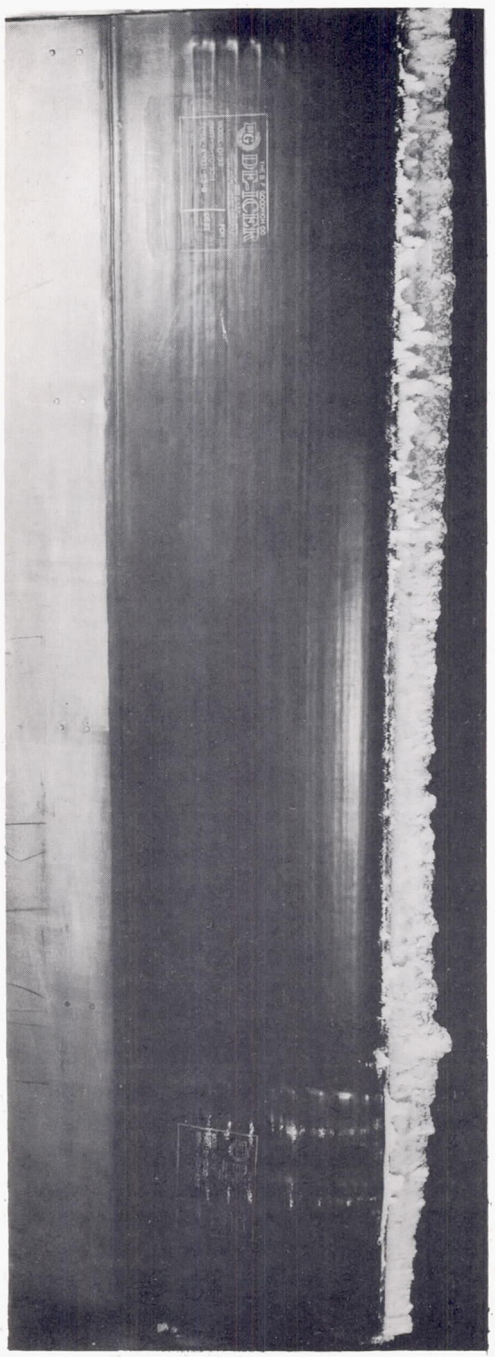

Upper surface

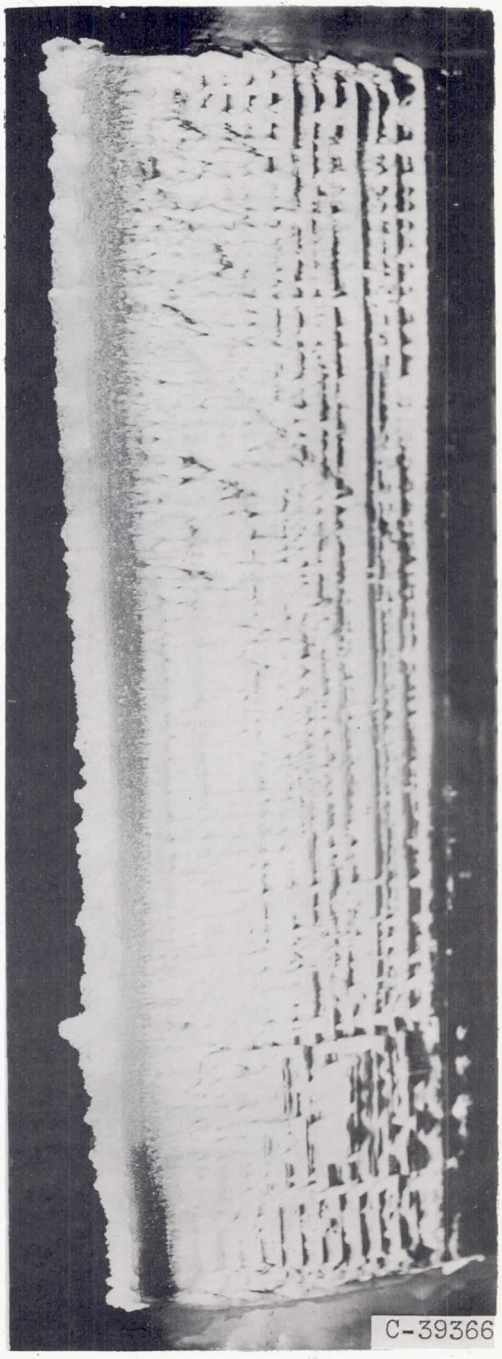

Lower surface

Figure 20. - Glaze-rime-ice formations on airfoil. Angle of attack, 9.3°; airspeed, 175 mph; total air temperature, 10° F; liquid-water content, 1.0 gram per cubic meter; icing time, 10 minutes; ice accumulation, 1.88 pounds per foot span; section drag coefficient, 0.0230; initial section drag coefficient, 0.0103; lift coefficient, 0.752; initial lift coefficient, 0.820.

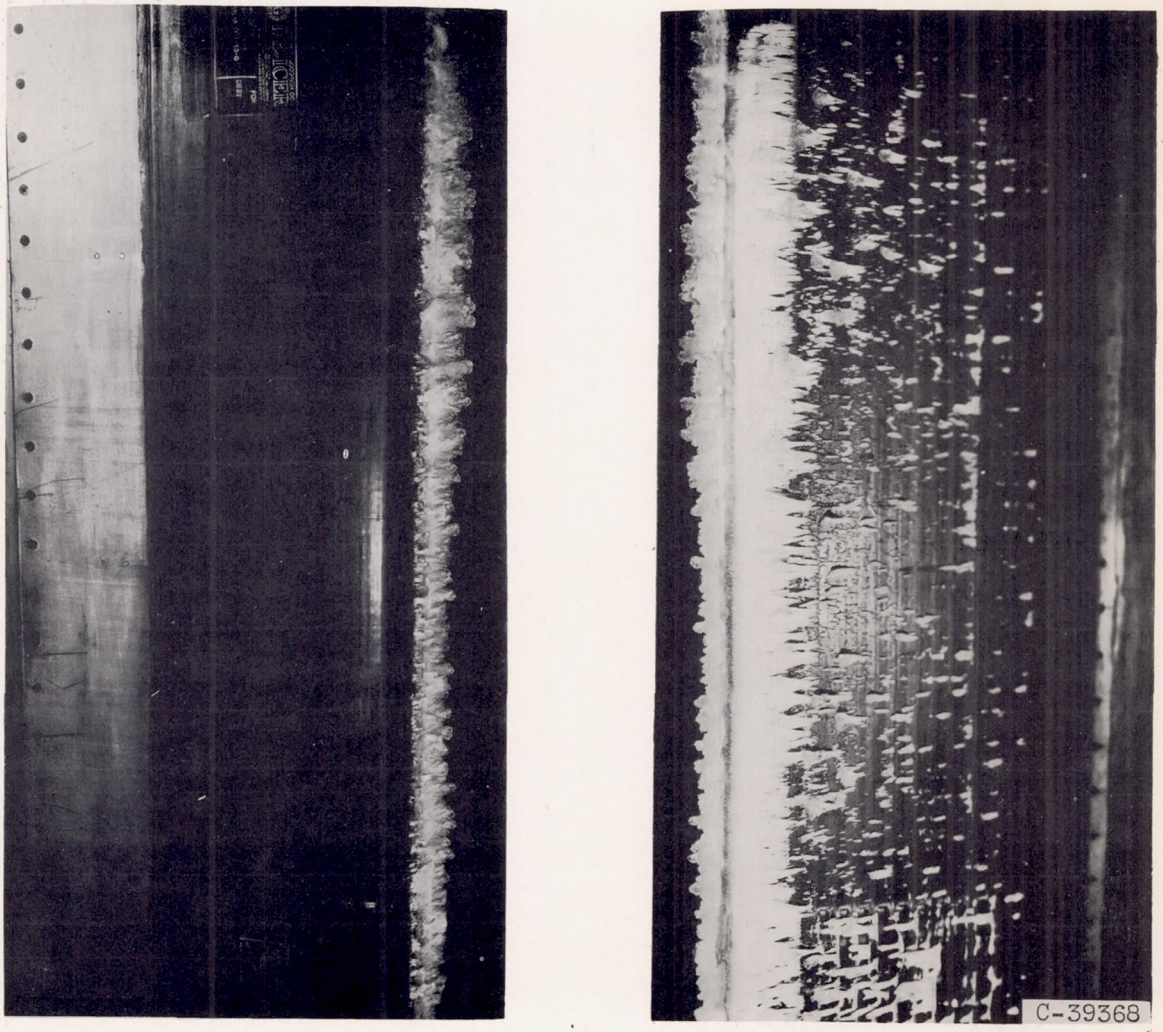

Upper surface Lower surface

Figure 21. - Typical glaze-ice formations on airfoil. Angle of attack, 7.0°; airspeed, 175 mph; total air temperature, 25° F; liquid-water content, 0.5 gram per cubic meter; icing time, 26 minutes; ice accumulation, 0.45 pound per foot span; section drag coefficient, 0.0127; initial section drag coefficient, 0.0087; lift coefficient, 0.592; initial lift coefficient, 0.613.

Upper surface

Lower surface

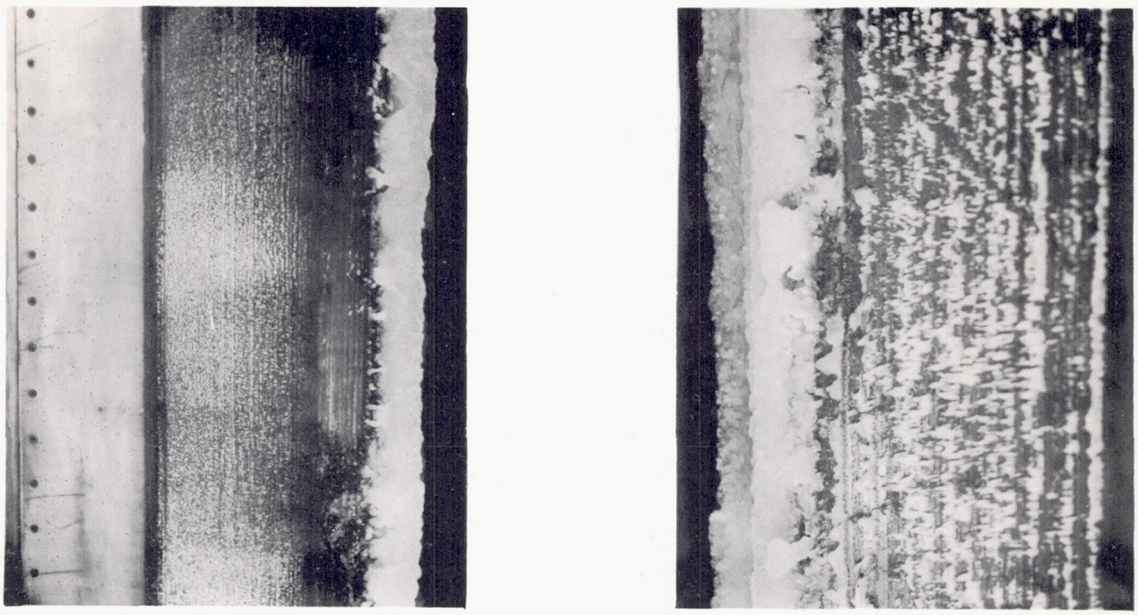

(a) Angle of attack, 2.3°; airspeed, 275 mph; liquid-water content, 0.5 gram per cubic meter; icing time, 18 minutes; ice accumulation, 0.81 pound per foot span; section drag coefficient, 0.0254; initial section drag coefficient, 0.0068; lift coefficient, 0.180; initial lift coefficient, 0.202.

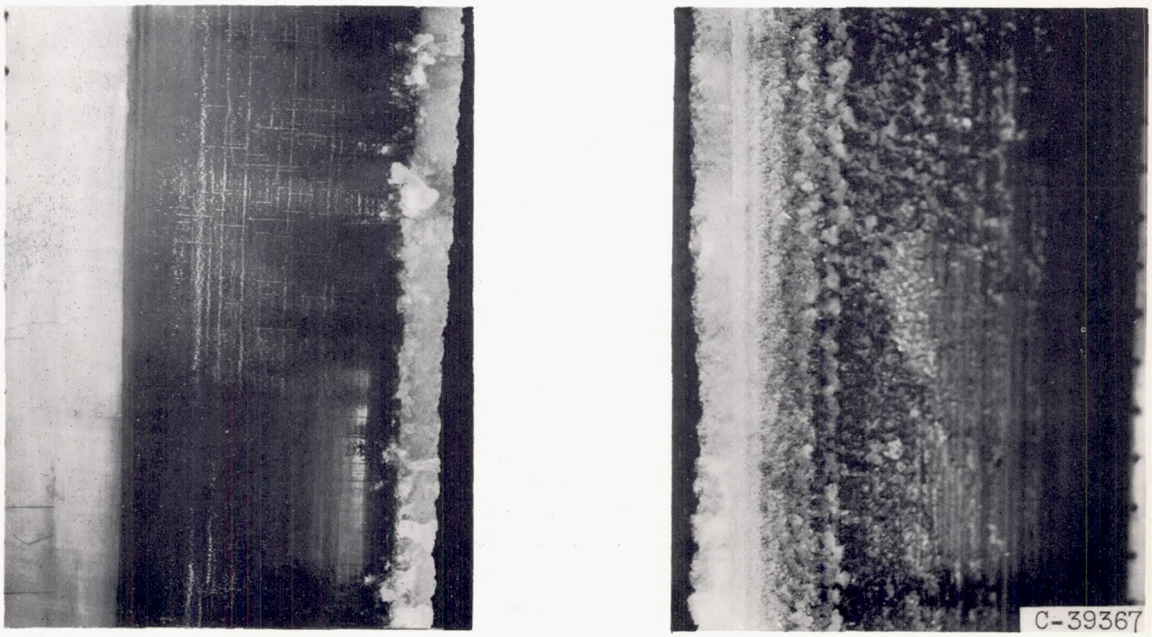

(b) Angle of attack, 7.0°; airspeed, 175 mph; liquid-water content, 1.0 gram per cubic meter; icing time, 10 minutes; ice accumulation, 0.73 pound per foot span; section drag coefficient, 0.0260; initial section drag coefficient, 0.0086; lift coefficient, 0.547; initial lift coefficient, 0.619.

Figure 22. - Typical ridge-type glaze-ice formations on airfoil. Total air temperature, 25° F.

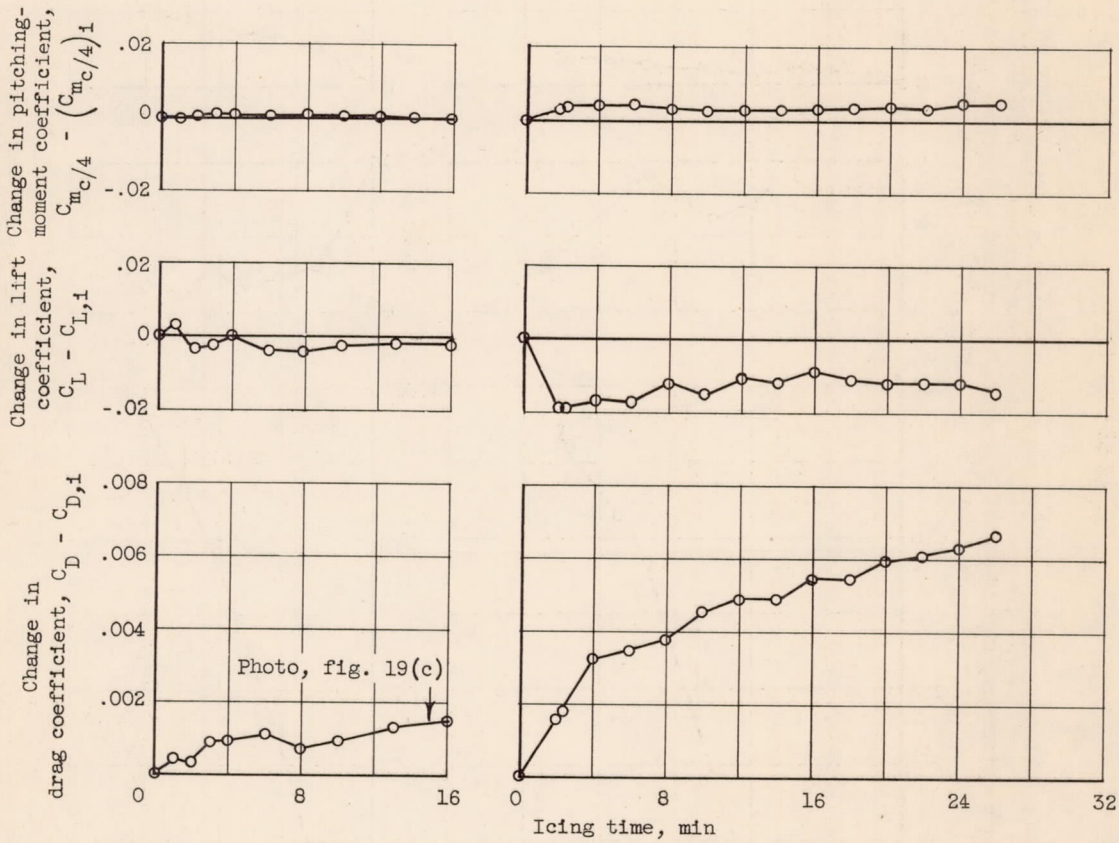

(a) Angle of attack, 2.3°; airspeed, 175 mph; initial lift coefficient, 0.194.

(b) Angle of attack, 4.6°; airspeed, 275 mph; initial lift coefficient, 0.419.

Figure 23. - Typical variation of section drag, lift, and pitching-moment coefficients with rime-ice formations on airfoil. Total air temperature, 10° F; liquid-water content, 0.5 gram per cubic meter; initial section drag coefficient, 0.0075.

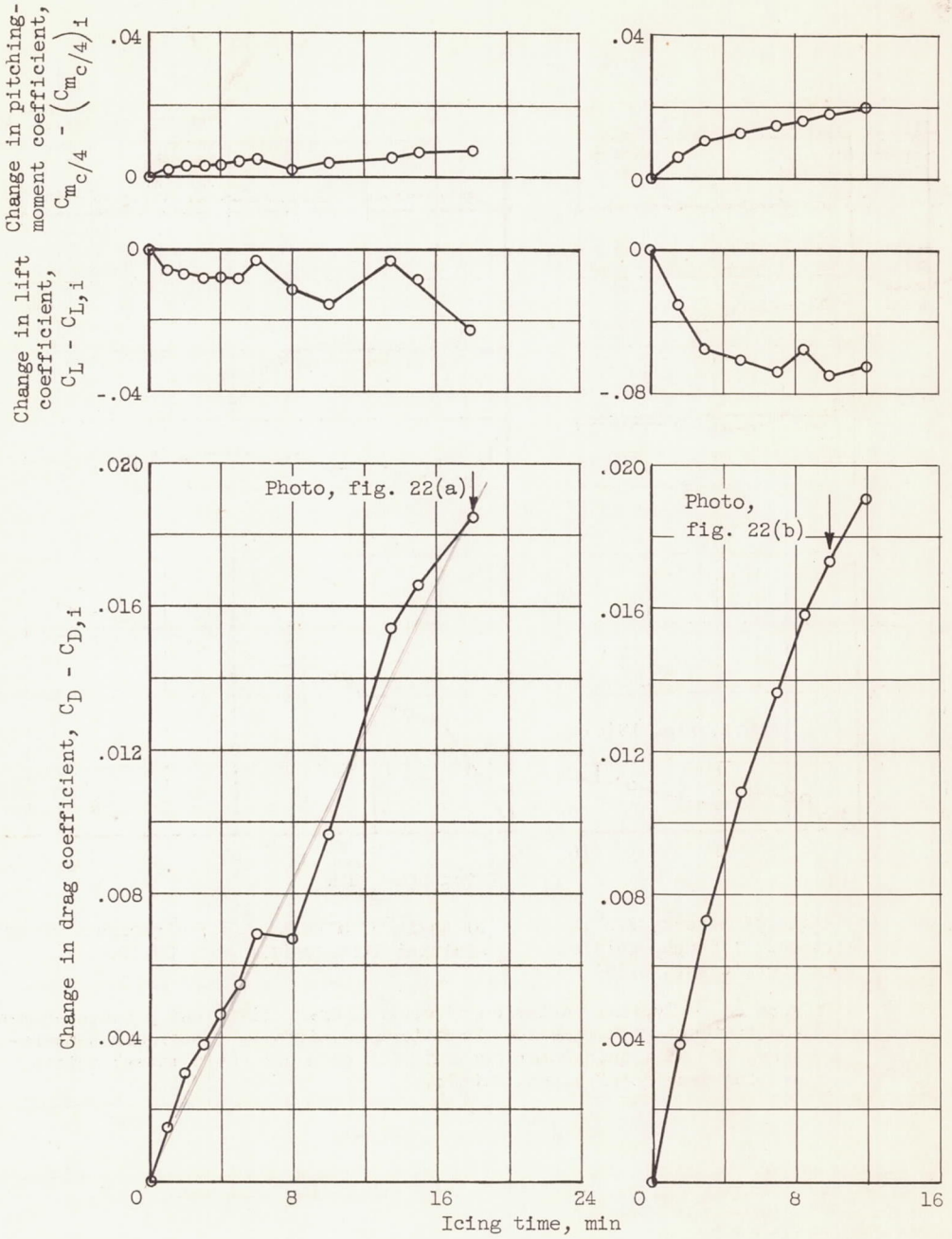

(a) Angle of attack, 2.3°; airspeed, 275 mph; liquid-water content, 0.5 gram per cubic meter; initial section drag coefficient, 0.0068; initial lift coefficient, 0.202.

(b) Angle of attack, 7.0°; airspeed, 175 mph; liquid-water content, 1.0 gram per cubic meter; initial section drag coefficient, 0.0086; initial lift coefficient, 0.619.

Figure 24. - Typical variation of section drag, lift, and pitching-moment coefficients with glaze-ice formations on airfoil. Total air temperature, 25° F.

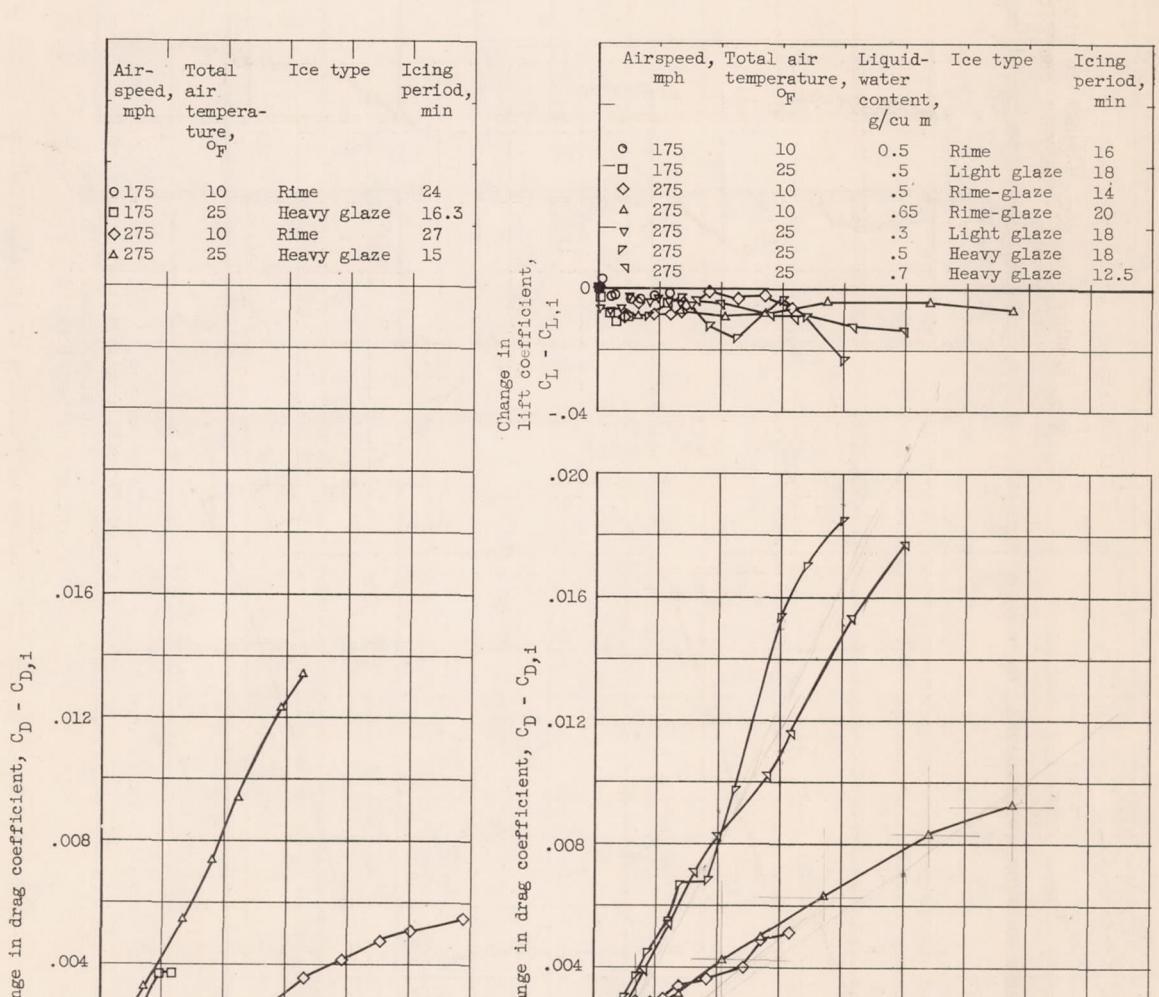

(a) Angle of attack, 0°; initial lift coefficient, 0; initial drag coefficient, 0.007; liquid-water content, 0.5 gram per cubic meter.

(b) Angle of attack, 2.3°; initial lift coefficient, 0.20; initial drag coefficient, 0.007.

Figure 25. - Airfoil section drag and lift changes as function of ice accumulation.

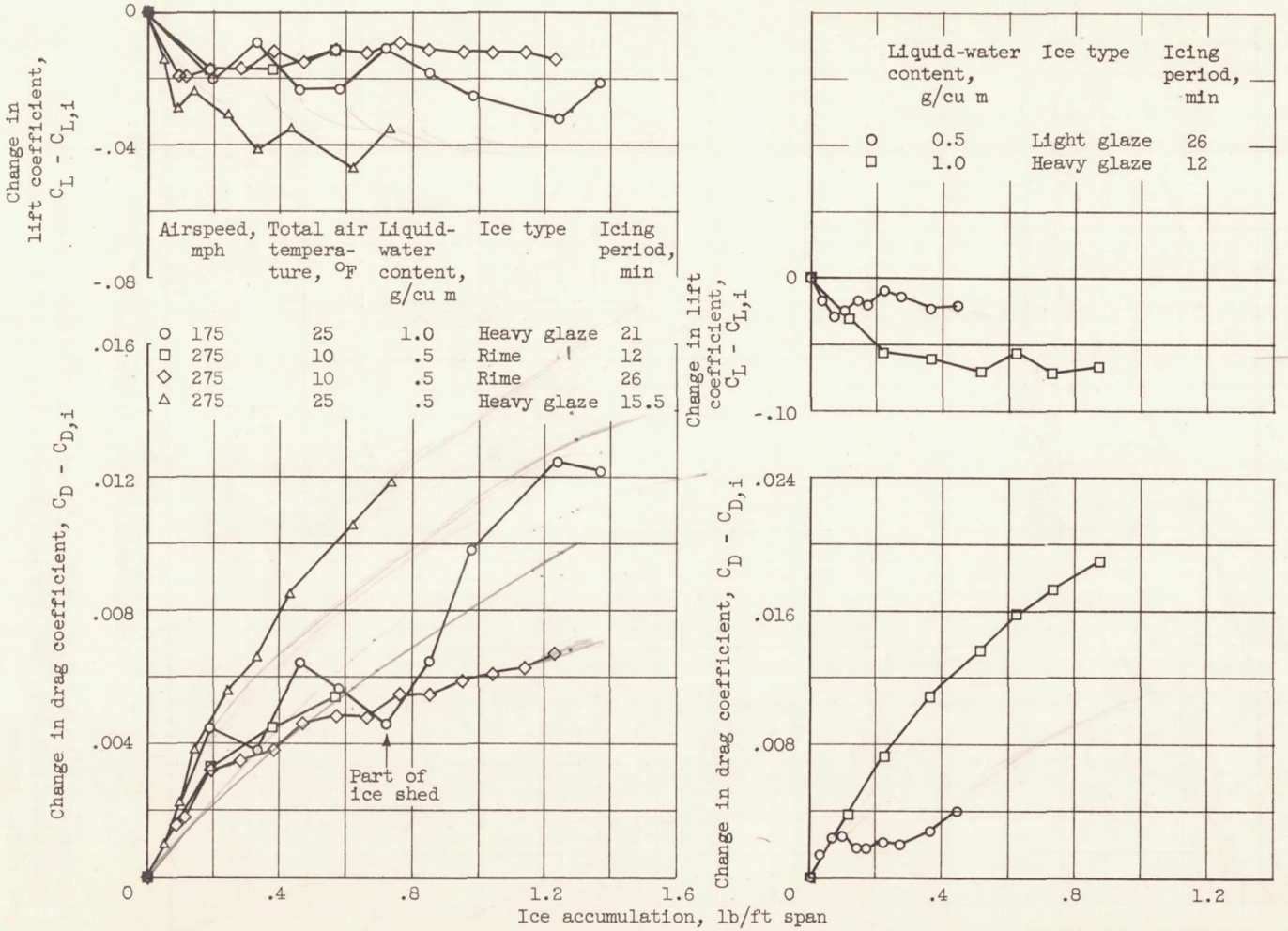

(c) Angle of attack, 4.6°; initial lift coefficient, 0.41; initial drag coefficient, 0.008.

(d) Angle of attack, 7.0°; initial lift coefficient, 0.61; initial drag coefficient, 0.009; airspeed, 175 mph; total air temperature, 25° F.

Figure 25. - Continued. Airfoil section drag and lift changes as function of ice accumulation.

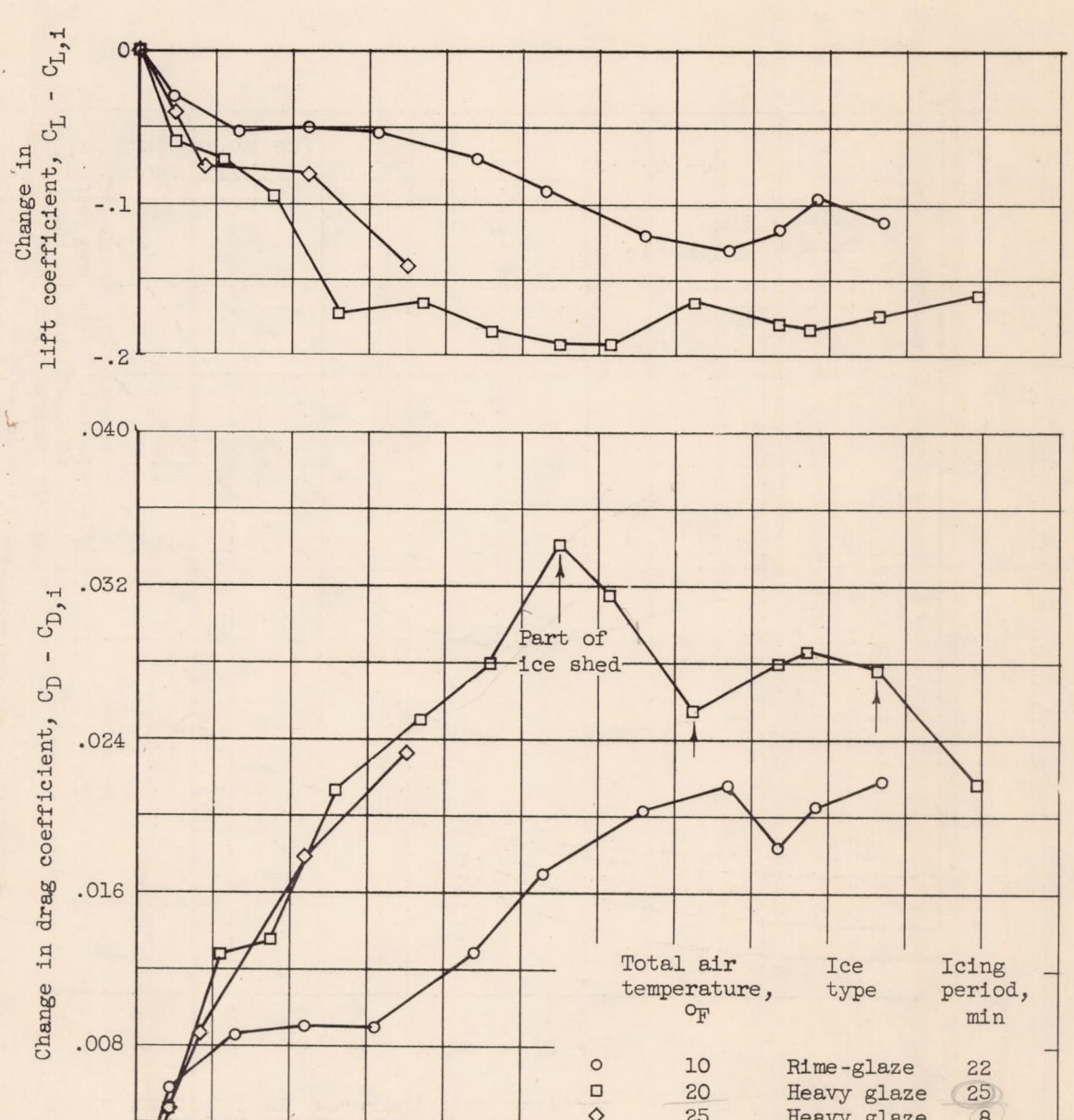

(e) Angle of attack, 9.3°; initial lift coefficient, 0.82; initial drag coefficient, 0.009; airspeed, 175 mph; liquid-water content, 1.0 gram per cubic meter.

Figure 25. - Concluded. Airfoil section drag and lift changes as function of ice accumulation.

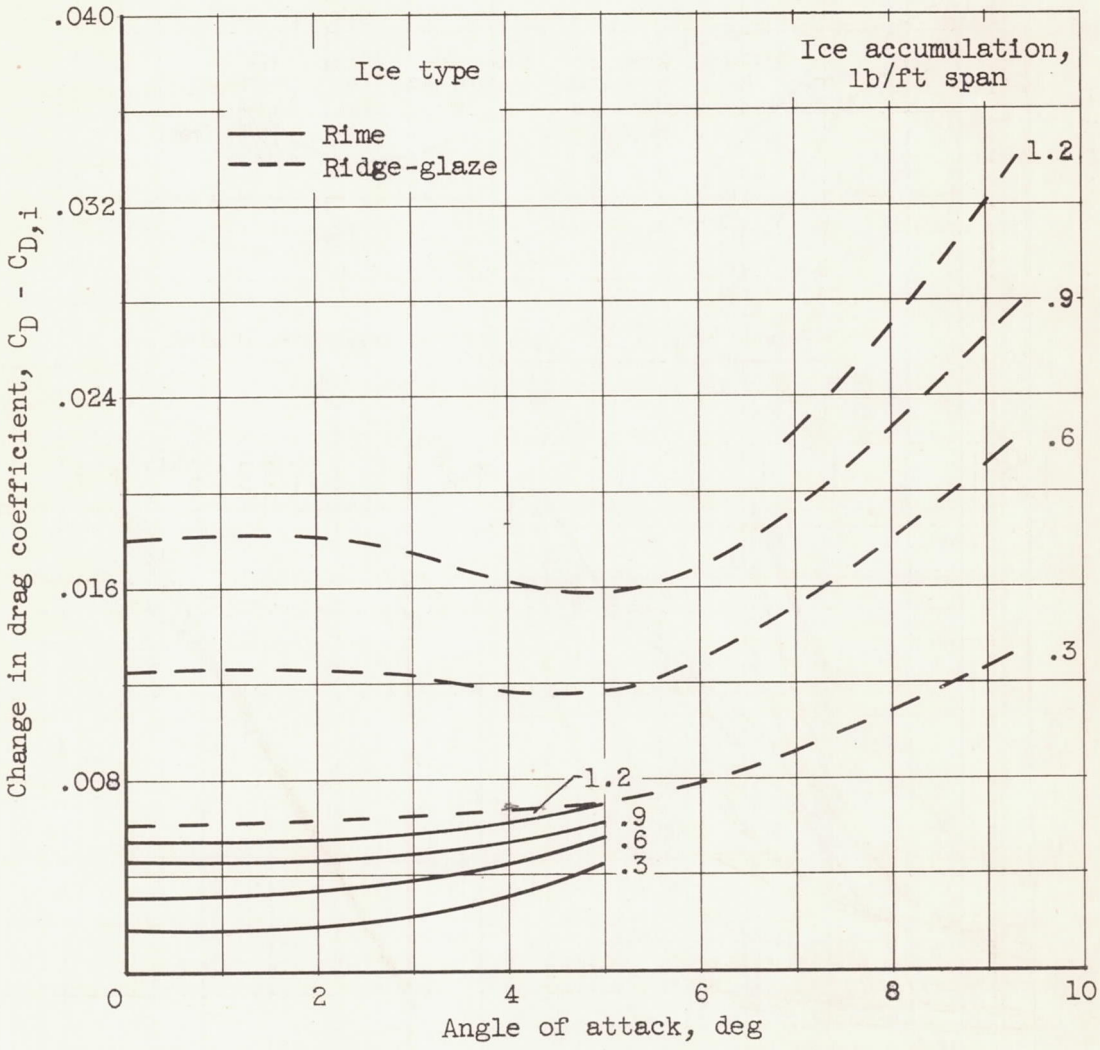

Figure 26. - Airfoil section drag increase as function of angle of attack for rime ice and ridge-type glaze ice.

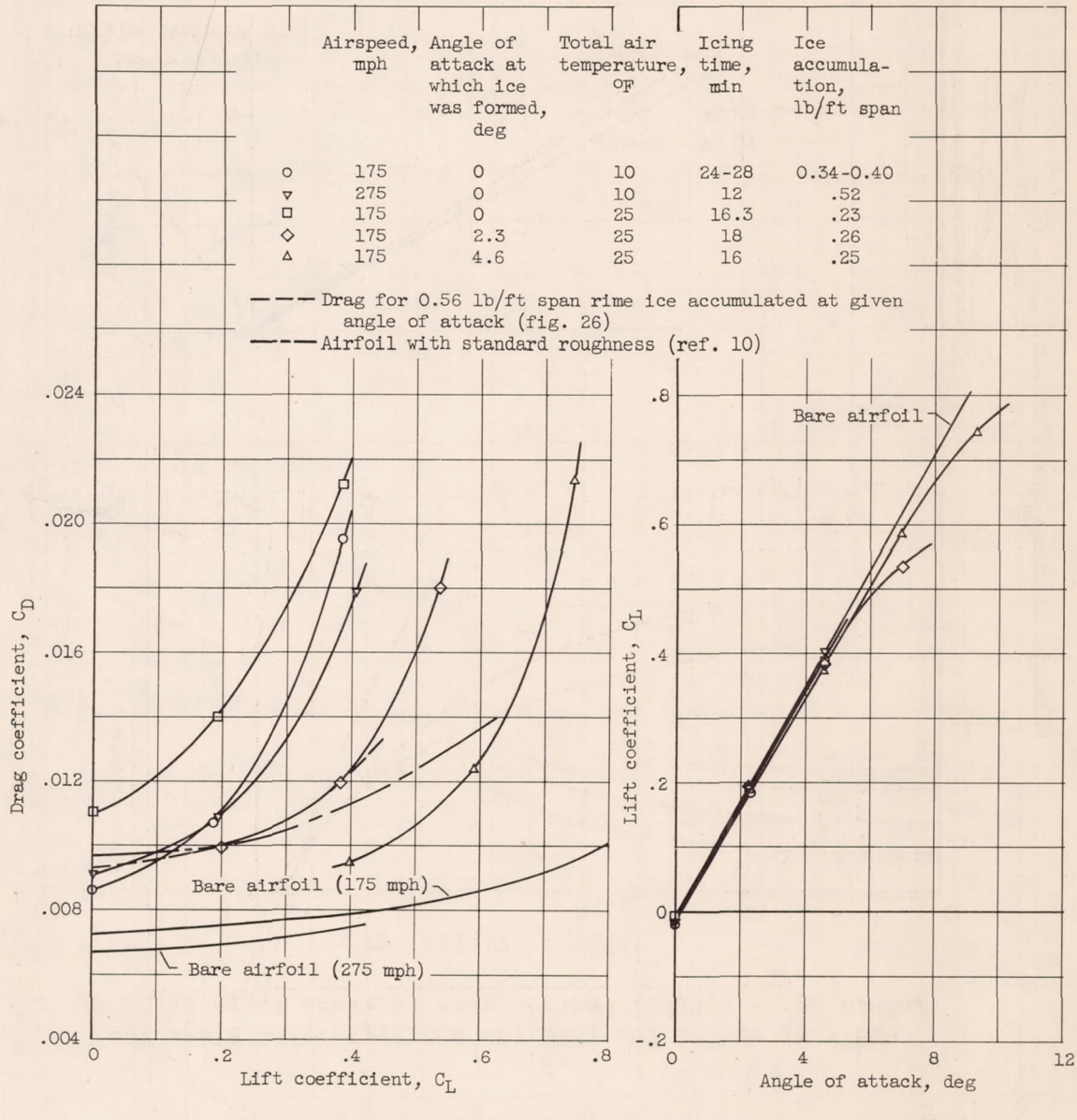

Figure 27. - Airfoil drag and lift changes caused by increasing angle of attack with ice on airfoil.

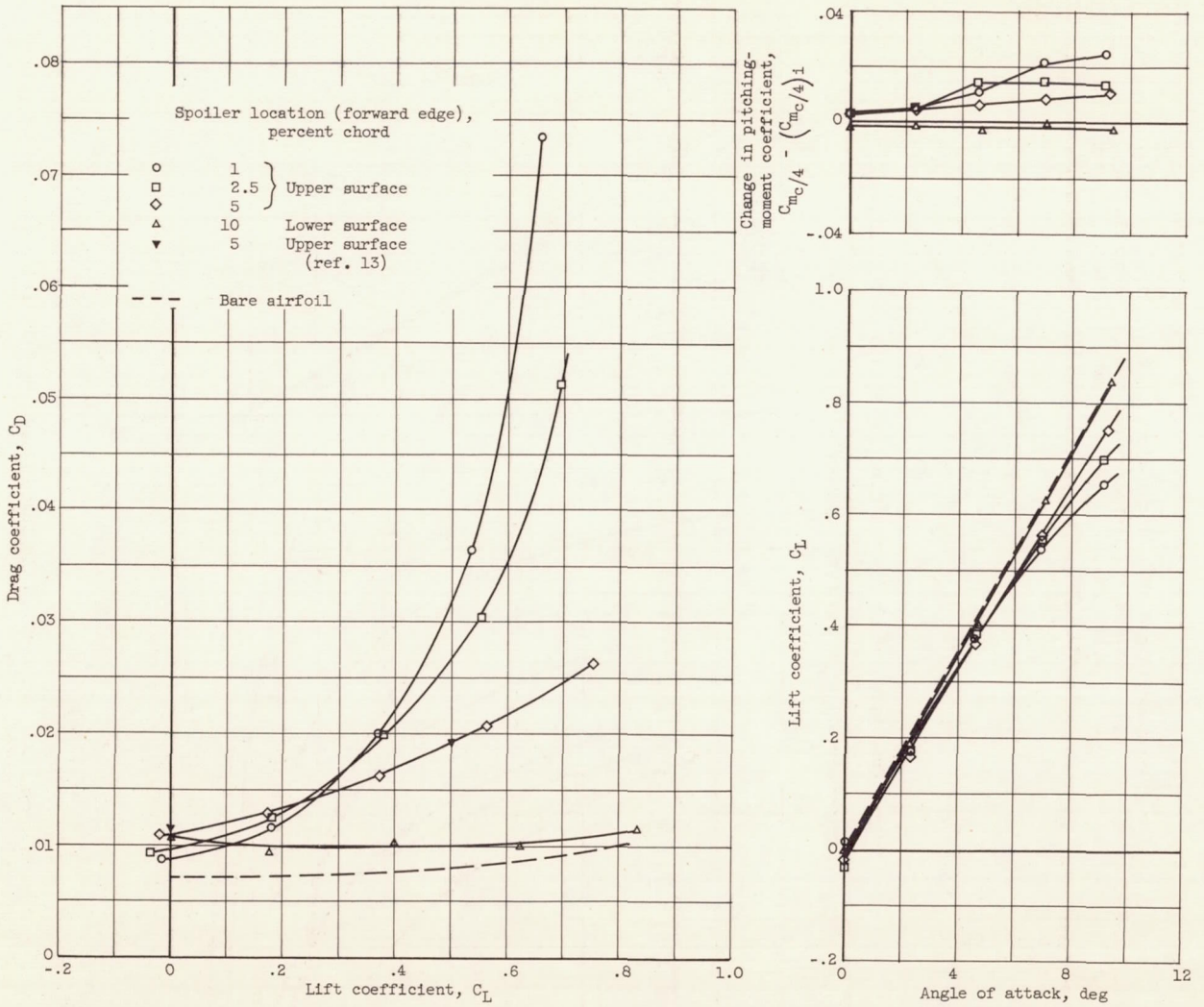

(a) 1/4-Inch-high spoilers (0.00286 chord).

Figure 28. - Airfoil section drag, lift, and pitching-moment coefficients with spanwise spoilers located at various chordwise positions.

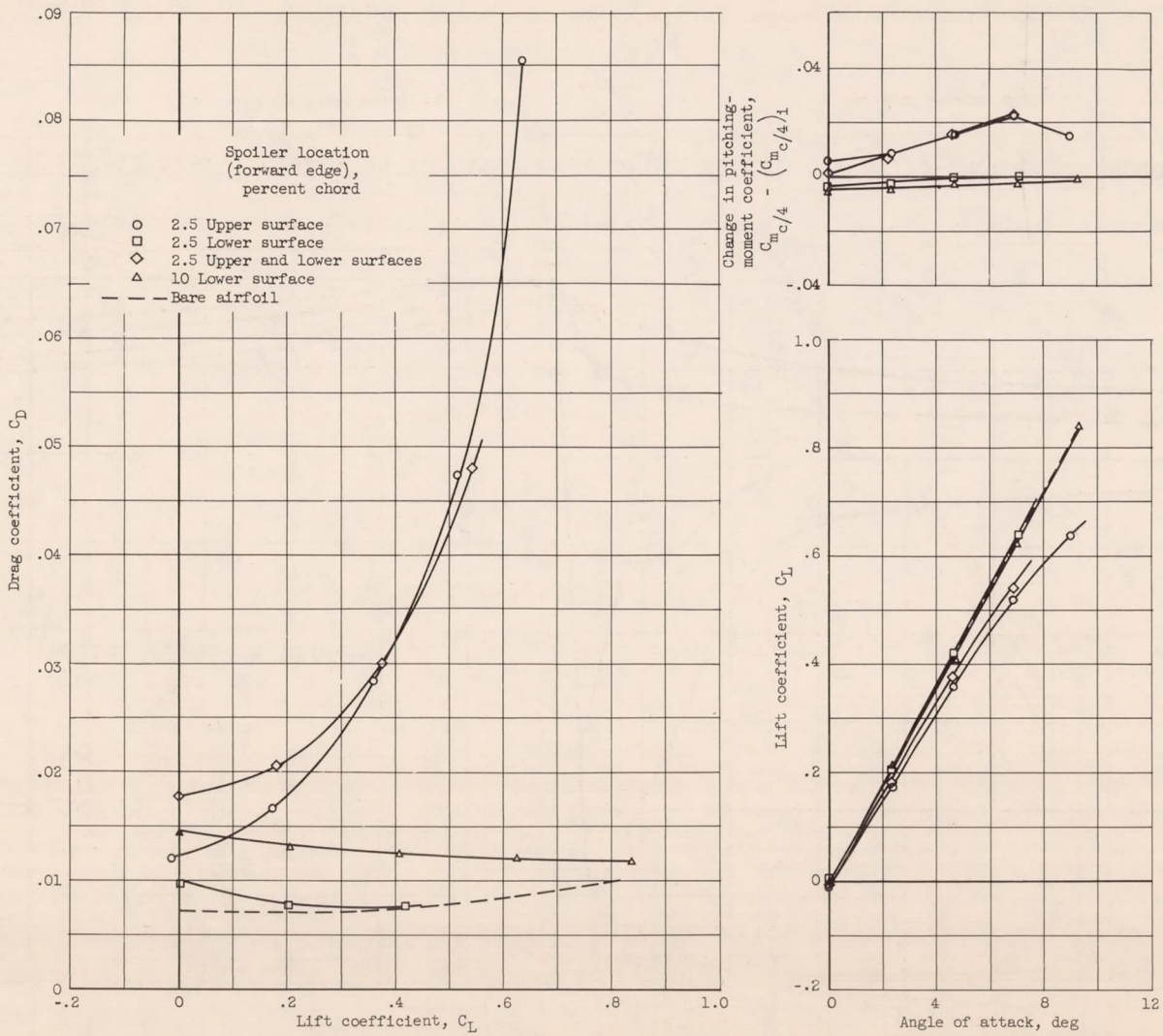

(b) 1/2-Inch-high spoilers (0.00572 chord).

Figure 28. - Concluded. Airfoil section drag, lift, and pitching-moment coefficients with spanwise spoilers located at various chordwise positions.

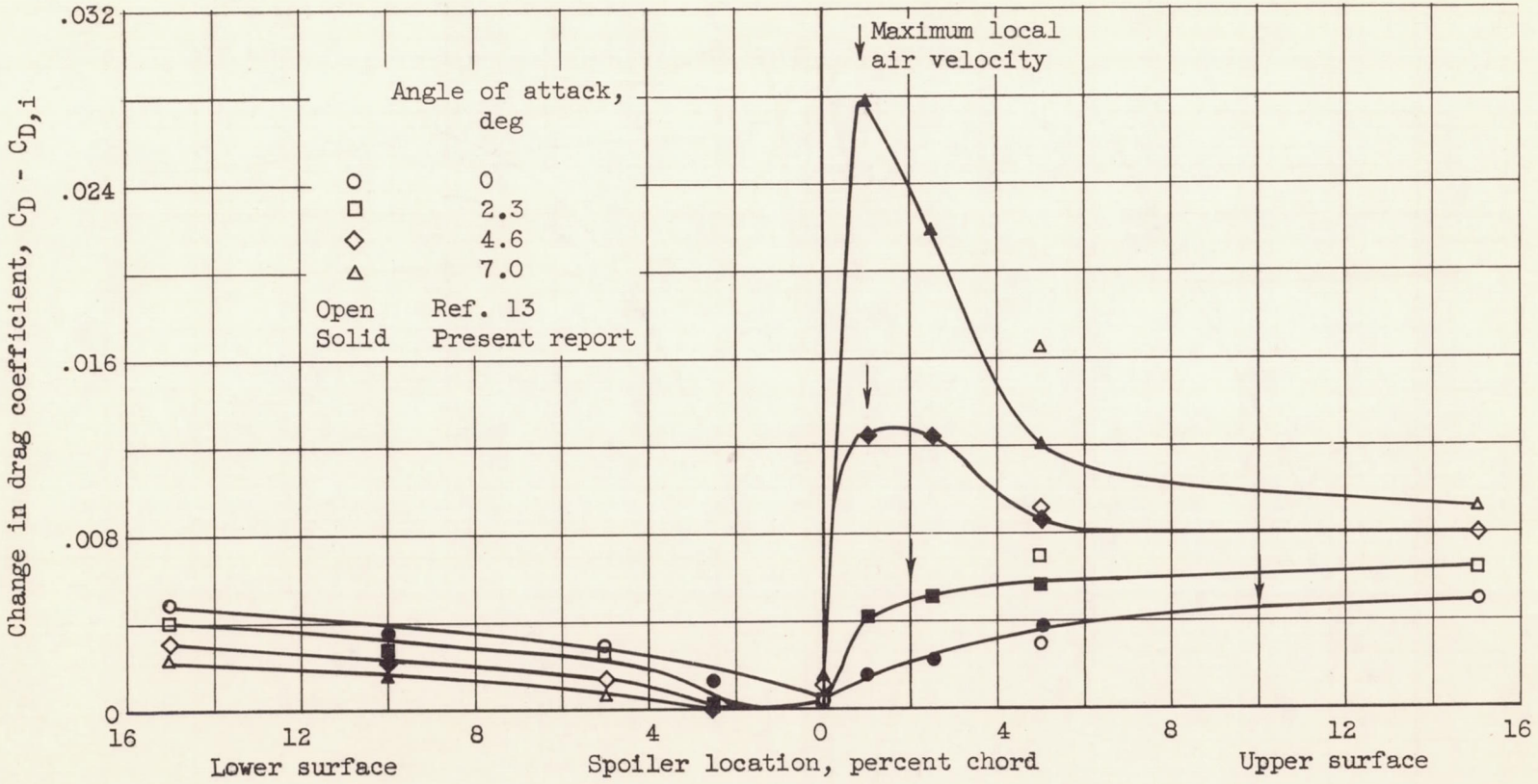

Figure 29. - Airfoil drag increase as function of spoiler location for 1/4-inch-high (0.00286 c) spoiler.

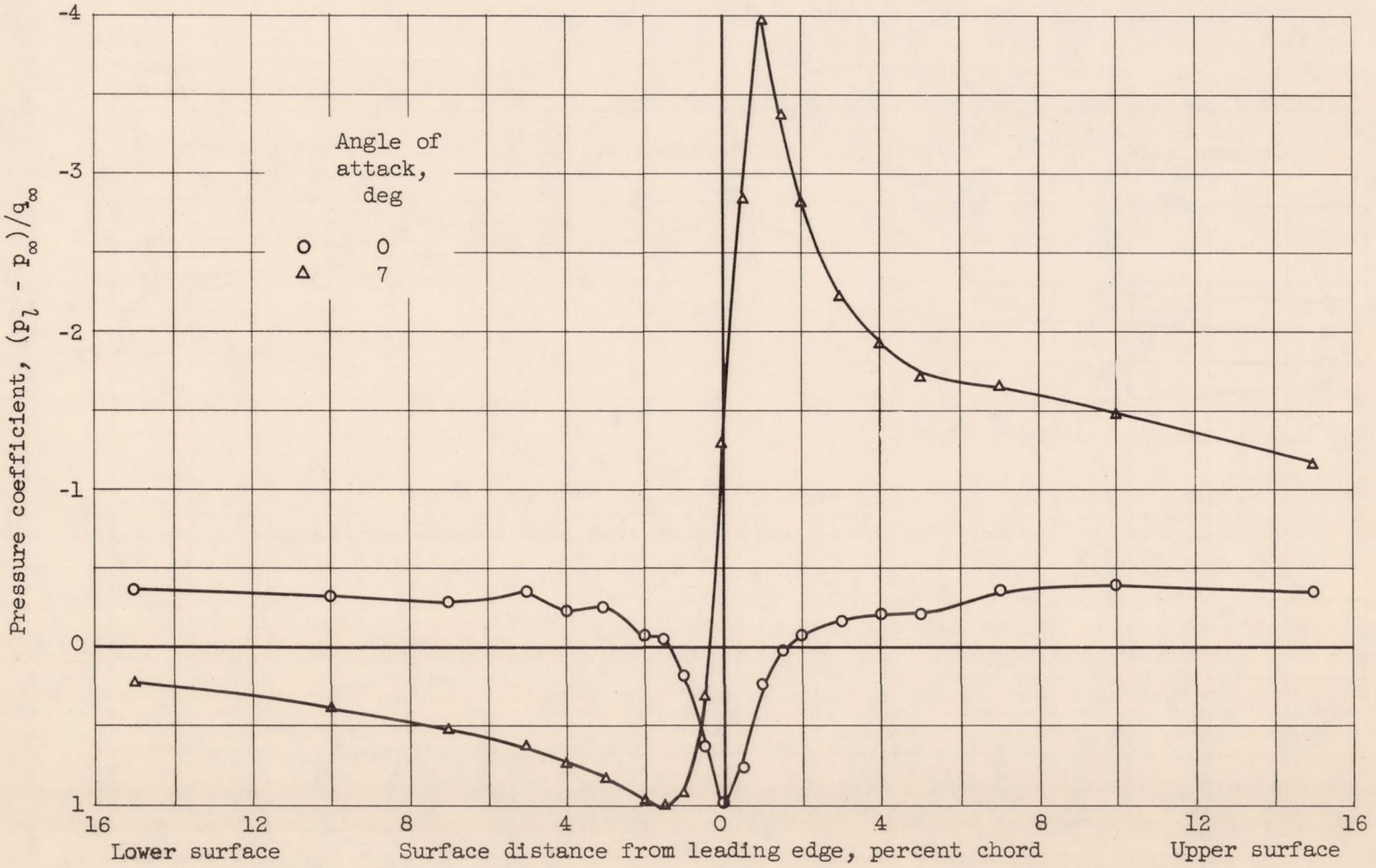

Figure 30. - Pressure distribution over bare airfoil leading-edge section.